Discovery of CHF-6523, an Inhaled Selective PI3Kδ Inhibitor for the Treatment of Chronic Obstructive Pulmonary Disease

AUTHORS

Paolo Bruno,[§,] Daniele Pala,[§] Alessandra Micoli,[Δ] Mauro Corsi,[Δ] Alessandro Accetta,[§] Laura Carzaniga,[§] Paolo Ronchi,[§] Claudio Fiorelli,[§] Michele Formica,[§] Daniela Pizzirani,[§] Roberta Mazzucato,[§] Sara Guariento,[§] Serena Bertolini,[§] Cataldo Martucci,[§] Andrew Dennis Allen,[§] Valentina Mileo,[§] Silvia Capacchi,[§] Paola Maria Gallo,[§] Alessandro Fioni,[§] Sergio Xanxo Fernandez,[§] Gino Villetti,[§] Paola Puccini,[§] Maurizio Civelli,[§] Matilde Guala,[Δ] Michele Retini,[Δ] Prisca Martinelli,[Δ] Filippo Visentini,[Δ] Valentina Pavoni,[Δ] Matteo Daldosso,[Δ] Stefano Fontana,[Δ] Matteo Biagetti,[§,*] Anna Maria Capelli.[§]*

[§]Chiesi Farmaceutici S.p.A, Centro Ricerche, Largo Belloli 11/a, 43122 Parma, Italy

[Δ]Aptuit, an Evotec Company, Via Alessandro Fleming, 4, 37135 Verona, Italy

KEYWORDS. PI3-kinases, PI3Kδ, Lung, Chronic respiratory diseases, Asthma, Chronic obstructive pulmonary disease (COPD), Inhaled drug, Pharmacokinetic, Ovalbumin, OVA.

ABSTRACT

The design of inhaled selective phosphatidylinositol 3-kinase delta (PI3Kδ) inhibitors for the treatment of inflammatory lung diseases was pursued. Knowledge-based design of a novel isocoumarin scaffold, able to adopt a *propeller-shape* topology, ensured the desired PI3Kδ selectivity. Achievement of low nanomolar cellular potencies through hinge binder group optimization, reduction of intrinsic permeability through head group optimization to extend lung retention, and screening of crystalline forms suitable for administration as dry powders culminated in the identification of compound **18**. This novel inhaled selective PI3Kδ inhibitor displayed durable anti-inflammatory activity in a disease relevant rat model of Th-2-driven acute lung inflammation and a safe *in vitro* and *in vivo* preclinical profile. Therefore, compound **18** showed the appropriate discovery profile and was progressed to clinical trials in healthy volunteers and chronic obstructive pulmonary disease (COPD) patients as CHF-6523.

INTRODUCTION

The management of severe asthma and of chronic obstructive pulmonary disease (COPD) exacerbations relies on the co-administration of long acting β_2 adrenergic agonist (LABA) bronchodilators, long acting muscarinic antagonist (LAMA) bronchodilators and inhaled corticosteroid (ICS) anti-inflammatory agents.[1,2] Notably, patients with COPD continue to experience exacerbations despite the availability of effective therapies, and evidence of resistance to ICSs has been reported both in asthma and in COPD patients.[3,4] This highlights the need of anti-inflammatory treatments to be administered on top of standard of care and targeting novel pathways, thus acting synergistically with inhaled corticosteroids.[5–11]

Phosphoinositide 3-kinase δ (PI3Kδ), is a lipid kinase expressed exclusively in leukocytes where it regulates activation, proliferation and function of multiple cell types, through phosphorylation of AKT:[12] crucially, the PI3Kδ pathway is upregulated in blood neutrophils and lung tissue derived from COPD patients.[9,13] Moreover, individuals with inherited activating mutations in PI3Kδ display profound immune defects.[14–16] As COPD exacerbations are often triggered by lung infections, PI3Kδ inhibitors may provide therapeutic benefit through their unique potential to improve neutrophil immune function by correcting the aberrant directionality of chemotaxis observed in COPD neutrophils[17] and by inhibiting inflammatory mediator release.[18] Both of these aspects of neutrophil function are not known to be addressed by corticosteroids. Moreover, bacterial and viral infections are among the most common causes of COPD exacerbations: since enhanced PI3Kδ signalling has been reported to increase susceptibility to *S. pneumoniae* infections,[19] inhibition of PI3Kδ stands out as an appealing therapeutic hypothesis to reduce exacerbations in COPD patients.

Over the years, several selective PI3Kδ inhibitors have been made available to patients for the oral treatment of oncological diseases (Idelalisib, Umbralisib, Figure 1a) and of activated PI3Kδ syndrome (APDS, Leniolisib, Figure 1a).[20] However, burdensome side-effects such as neutropenia, thrombocytopenia, anemia, transaminitis, diarrhea, colitis and pneumonia have been reported following the oral administration of PI3Kδ inhibitor drugs.[21,22] Conversely, treatment of respiratory diseases could take advantage of administration of therapeutic agents by inhalation, resulting in high drug concentrations in the lungs to elicit desired therapeutic effect, and largely reduced systemic exposure to minimize side effects outside the respiratory tract. Notably, administration of selective PI3Kδ inhibitors by inhalation has been pursued in clinical trials (Nemiralisib, GSK2292767, Figure 1b).[20]

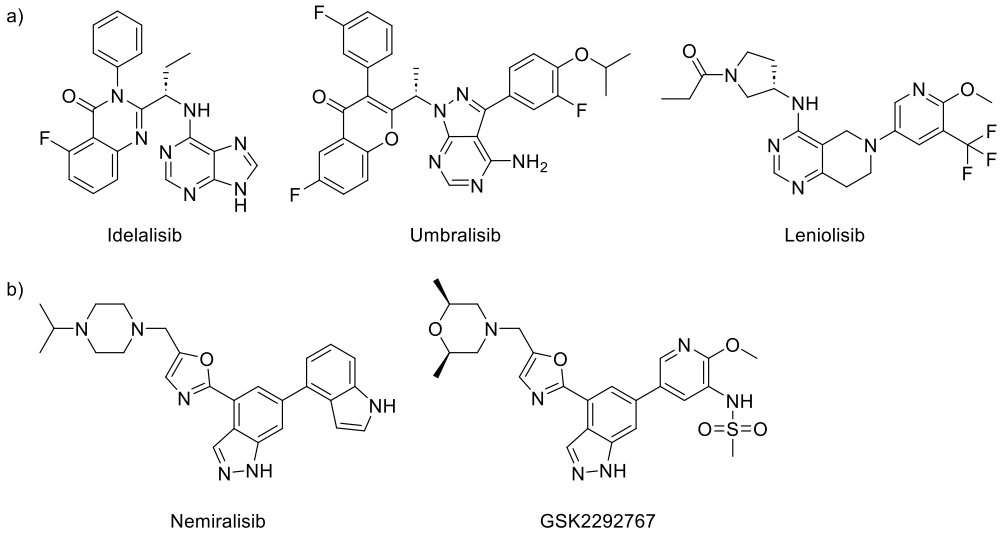

Figure 1. a) Approved orally administered selective PI3Kδ inhibitors; b) inhaled selective PI3Kδ inhibitors progressed to clinical trials.

Coherently with the aim of minimizing side effects, we envisaged the optimization of novel PI3Kδ inhibitors for delivery by inhalation. Advantageously, inhaled PI3Kδ drugs could theoretically be co-administered with ICSs through a single device, similarly to available LABA+ICS double– and LABA+LAMA+ICS triple–fixed combinations,[2] thus purposely

facilitating compliance to therapy. Besides pursuing administration by inhalation to minimise PI3Kδ-related systemic side-effects, selectivity toward other PI3K isoforms[23] was sought. Specifically, we aimed at minimal inhibition of PI3Kα and PI3Kβ isoforms in order to stay clear of unwanted effects such as hyperglycemia[24] or embolization.[25]

The objective of our work was to find an answer to the inflammatory component of chronic lung diseases through modulation of PI3Kδ signalling pathways, a condition not addressed by current standard of care. The drug discovery program involved the design of a novel isocoumarin series of PI3Kδ selective inhibitors, among which a series of optimizations to improve compound's developability for administration by inhalation resulted in the identification of the clinical candidate CHF-6523.

RESULTS AND DISCUSSION

Hit Identification: Selective PI3Kδ Ligands Design.

Selectivity requirements directed the design of new scaffolds toward moieties able to adopt the *propeller-shape* conformation adopted by Idelalisib upon binding to PI3Kδ (Figure 2a). This conformation is responsible of an induced fit in PI3K binding pockets, caused by the displacement of the side chain of a methionine residue in the P-loop (Met-752 in PI3Kδ) and by movement of the P-loop itself, ultimately resulting in the opening of the so-called *specificity pocket*. Differently from PI3Kα and PI3Kβ, this conformational change can be conveniently adopted by PI3Kδ enzyme on account of the higher flexibility of its P-loop, making propeller-shape inhibitors more selective for PI3Kδ.[26]

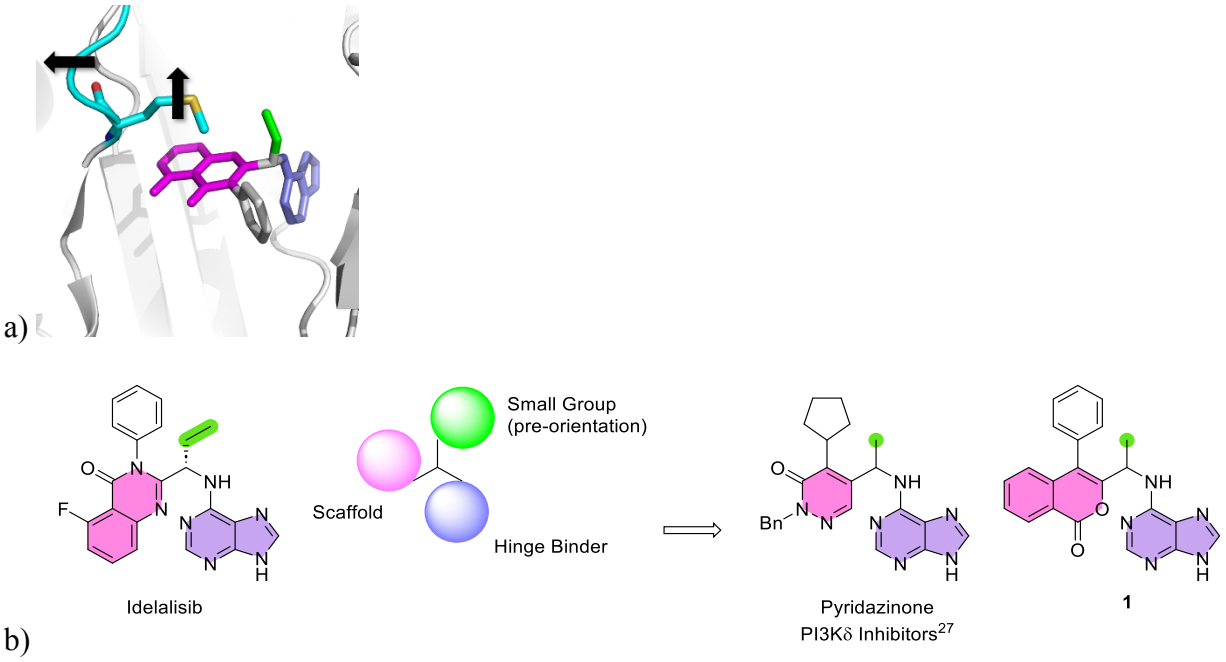

Figure 2. a) Idelalisib bound to hPI3Kδ (pdb 4XE0); b) topology of propeller-shaped inhibitors and novel scaffolds designed.[27]

In light of this consideration, Idelalisib was selected as a template for the design of novel PI3Kδ inhibitors. In particular, the small alkyl group (highlighted in green in Figure 2b) favoring the adoption of *propeller-shape* conformation, as well as the hinge binder group (purple) were retained. Conversely, modifications of the quinazolin-4(*3H*)-one scaffold of Idelalisib were conceived, such as (i) the deconstruction of the bicyclic system, leading to the monocyclic scaffold of previously disclosed pyridazinone PI3Kδ inhibitor series (Figure 2b),[27] or (ii) the modification of the topology of Idelalisib's quinazolin-4(*3H*)-one scaffold to scope slightly different portions of the *specificity pocket*,[26] leading to isocoumarin core embedded into compound **1** (Figure 2b). Enzymatic activity of compound **1** was measured on the four PI3Ks belonging to classes IA and IB[23] by means of ADP-Glo™ assay in human (h) recombinant kinases hPI3Kα (p110α/p85α), hPI3Kβ (p110β/p85α), hPI3Kδ (p110δ/p85α) and hPI3Kγ (p110γ)[28] and compound inhibitory activity was expressed as pK_i value (see Experimental Part).

Pleasingly, compound **1** displayed a promising enzymatic PI3K inhibition profile, being comparable both to approved oral drug Idelalisib and importantly also to GSK2292767, an inhaled selective PI3Kδ inhibitor that was administered in clinical trials as a dry powder (ClinicalTrials.gov ID NCT03045887). Specifically, compound **1** displayed a pK_i of 8.4 on PI3Kδ isoform along with higher than 150–fold selectivity over PI3Kα and β (Table 1), thus it was progressed to cell-based PI3Kδ inhibition assay. In this test, the PI3Kδ/AKT pathway is stimulated in THP-1 monocytes by application of Macrophage Colony-Stimulating Factor (M-CSF) and the resulting AKT phosphorylation is then measured through Homogeneous Time Resolved Fluorescence (HTRF) technology (see Experimental Part).[29] Inhibition of cell fluorescence exerted by tested compound is expressed as pIC_{50} value, representing compound's potency. Sub-micromolar activity was measured for compound **1** (6.6 pIC_{50}, Table 1), demonstrating that this hit compound could retain potency in a cell-based setting, and highlighting a key driver for optimization. As a matter of fact, high potency, ideally in the low nanomolar range, is mandatory for inhaled drugs due to limitations on maximal amount of drug that can be administered by the inhalatory route both to animals in *in vivo* pharmacodynamic (PD) models and to patients.

Table 1. *In Vitro* PI3K Inhibition Data of Compound **1** in Comparison with Idelalisib and GSK2292767.

Compound	PI3Kδ pK_i[a]	PI3Kγ pK_i[a]	PI3Kβ pK_i[a]	PI3Kα pK_i[a]	THP-1 pIC_{50}[a]
Idelalisib[b]	8.8 ± 0.03	7.6 ± 0.03	7.2 ± 0.09	6.4 ± 0.10	7.5 ± 0.06
GSK2292767[c]	9.1 ± 0.04	7.6 ± 0.04	7.3 ± 0.05	7.5 ± 0.06	8.4 ± 0.29
1	8.4 ± 0.04	7.3 ± 0.05	6.2 ± 0.11	5.6 ± 0.10	6.6 ± 0.15

[a]Data expressed as mean ± standard deviation of two independent determinations each in duplicate.

[b]Supplied for research use only by MedChemExpress, item catalog number HY-13026. *In vitro* profile of Idelalisib is in good agreement with published PI3Kδ inhibition data.[30] Differences of values with respect to literature can be ascribed to differences in experimental conditions used.

[c]Supplied for research use only by MedChemExpress, item catalog number HY-15280. *In vitro* profile of GSK2292767 is in good agreement with published PI3Kδ inhibition data.[31] Differences of values with respect to literature can be ascribed to differences in experimental conditions used.

Hit Optimization: Improving PI3Kδ Cellular Potency.

Having demonstrated that newly designed isocoumarin scaffold can achieve a good enzymatic PI3Kδ potency and selectivity profile, we tackled optimization of cellular potency by scoping chemical diversity at other portions of compound **1**, in particular leveraging both on the wealth of hinge binder groups available in the literature[32] and on new designs by our side. More than 90 analogues of compound **1**, comprising mono– and bicyclic hinge binders of different topologies, with and without the addition of the so-called *affinity group*[28] (Figure 3), were prepared and tested in the enzymatic assay. Specifically, *affinity groups* were inserted onto hinge binders in order to occupy the *affinity pocket*, a region deep in PI3K binding pocket which is not accessed by ATP and lies between gatekeeper residue Ile-879 and Asp-911 belonging to DFG motif. In particular, aromatic *affinity groups* were selected to establish apolar interactions with Ile-879, while polar decorations were inserted on them with the purpose of binding to Asp-911 and other polar residues in the *affinity pocket*.

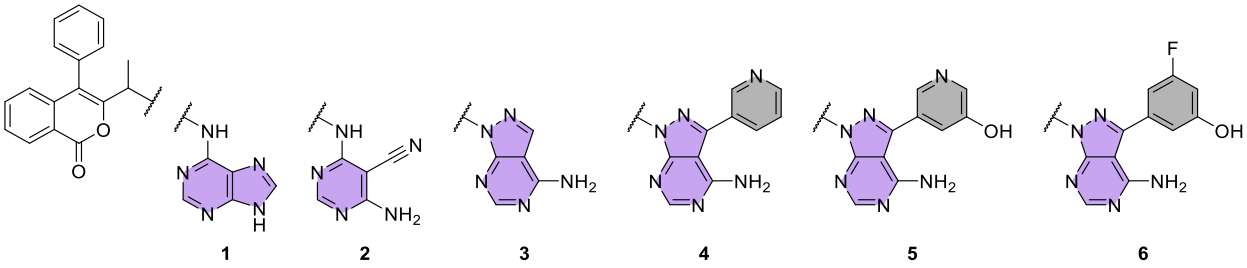

Figure 3. Representative structures of hinge binders (purple) and hinge binder-*affinity group* (gray) combinations.

Inhibition of PI3Kδ, α and β measured in enzymatic assay confirmed that the newly designed scaffold was conducive to potent and selective PI3Kδ inhibitors across a good number of hinge binders screened (green dots in upper-right green box in Figure 4a). Potent and selective compounds in enzymatic assay were then progressed to cell-based assay, where low nanomolar potencies (pIC_{50} >8.5, upper green box in Figure 4b) were achieved, with higher than 80–fold improvement over first hit compound **1**.

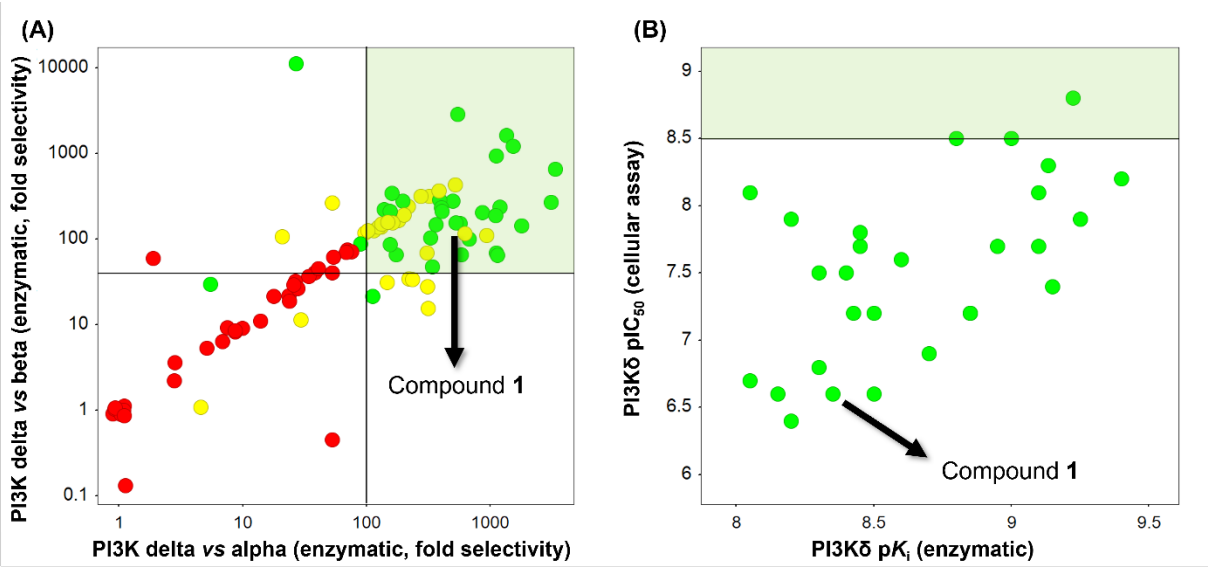

Figure 4. a) Enzymatic PI3Kδ/β fold selectivity *vs* PI3Kδ/α fold selectivity. b) PI3Kδ cellular pIC_{50} *vs* enzymatic pK_i. Color coding according to PI3Kδ enzymatic potency: pK_i <7.0 red; 7.0< pK_i <8.0 yellow; pK_i >8.0 green.

Detailed structure-activity relationship (SAR) analysis identified key drivers for enzymatic and cellular PI3Kδ inhibitory potency. A shift from bicyclic hinge binder of compound **1** to simpler monocyclic hinge binder of compound **2** (Figure 3) resulted in slightly higher, though still sub-

optimal cellular potency (Table 2). A set of sequential structural modifications, namely (i) hinge binder topology change (compound **3**, Figure 3), (ii) *affinity group* addition (compound **4**, Figure 3), and (iii) hydroxyl group insertion onto *affinity group* (compound **5**, Figure 3), proved synergistically successful in achieving desired low nanomolar cellular potencies in THP-1 assay.

Table 2. Biological Data of Compounds Scoping Diverse Hinge Binders and *Affinity Groups*.

Compound	PI3Kδ pK_i[a]	PI3Kγ pK_i[a]	PI3Kβ pK_i[a]	PI3Kα pK_i[a]	THP-1 pIC_{50}[a]
1	8.4 ± 0.04	7.3 ± 0.05	6.2 ± 0.11	5.6 ± 0.10	6.6 ± 0.15
2	8.9 ± 0.08	7.3 ± 0.01	5.7 ± 0.01	5.7 ± 0.07	7.2 ± 0.05
3	7.2 ± 0.09	5.7 ± 0.02	< 4.7	< 4.7	n.t.[b]
4	7.0 ± 0.02	6.1 ± 0.09	< 4.7	< 4.7	n.t.[b]
5	9.0 ± 0.03	7.4 ± 0.07	7.1 ± 0.01	6.3 ± 0.05	8.5 ± 0.16
6	9.1 ± 0.01	7.7 ± 0.01	6.8 ± 0.01	6.1 ± 0.02	7.8 ± 0.04

[a]Data expressed as mean ± standard deviation of two independent determinations each in duplic

[b]Compound not tested.

Suitably optimized enzymatic PI3Kδ selectivity and cellular potency of racemic compound **5** prompted isolation of single enantiomers, allowing identification of eutomer **7** (Table 3).

Table 3. Biological Data of Single Enantiomers Isolated from Compound **5**.

Compound	Absolute stereochemistry	PI3Kδ pK_i[b]	PI3Kγ pK_i[b]	PI3Kβ pK_i[b]	PI3Kα pK_i[b]	THP-1 pIC_{50}[b]
5	racemic	9.0 ± 0.03	7.4 ± 0.07	7.1 ± 0.01	6.3 ± 0.05	8.5 ± 0.16
7	(*S*)[a]	9.2 ± 0.10	8.1 ± 0.16	7.5 ± 0.07	6.7 ± 0.03	8.8 ± 0.22
8	(*R*)	7.5 ± 0.06	5.9 ± 0.07	6.0 ± 0.08	< 4.7	n.t.[c]

[a]Absolute stereochemistry was attributed in agreement with previously disclosed, topologically similar PI3Kδ inhibitor[27] and with Idelalisib.

[b]Data expressed as mean ± standard deviation of two independent determinations each in duplicate.

[c]Compound not tested.

A visual inspection of the best-ranked docking pose of compound **7** shed light on the pivotal role of a hydroxyl group suitably placed on the pyridine ring *affinity group*, proving that this moiety is involved in a network of hydrogen bonds with backbone nitrogen of Asp-911 and with side chain polar groups of residues Asp-787 and Tyr-813 (Figure 5). Nanomolar PI3Kδ inhibitory potency of compound **6** (Figure 3, Table 2), which embedded 3-fluorophenol *affinity group*,[26] demonstrated the general beneficial effect on potency of the hydroxyl group.

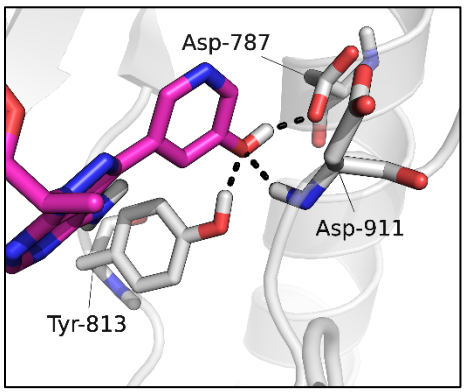

Figure 5. Detail of H-bond network between the 3-hydroxypyridine *affinity group* of compound **7** (magenta carbons) and hPI3Kδ kinase residues.

Hit-to-Lead: *in vitro* ADME-*in vivo* PK correlation.

Being PI3Kδ enzymatic selectivity and cellular potency of compound **7** in desired range, characterization in a panel of PhysChem and *in vitro* absorption, distribution, metabolism and excretion (ADME) assays followed (Table 4, see Experimental Part for detailed description of assays). High stability in lung S9 fraction and medium intrinsic permeability looked supportive of slow clearance from lung following administration by inhalation, while medium to short half-

lives ($t_{1/2}$) in hepatic microsomes and hepatocytes looked promising in view of desired rapid clearance from systemic circulation. Accordingly, profile of compound **7** was considered acceptable in view of progression to *in vivo* pharmacokinetic (PK) studies to build *in vitro-in vivo* correlations and establish whether any optimization was necessary.

Table 4. ADME, PhysChem and Calculated Properties of Compound **7**.

Property	Value
Lung S9 $t_{1/2}$	>146 min (h) – >146 min (r)[a]
Hepatic Microsomes $t_{1/2}$[b]	40 min (h) – 14 min (r)
Hepatocytes $t_{1/2}$[c]	25 min (h) – 7.6 min (r)
Intrinsic permeability (Caco-2 $P_{app}AB$[d])	43 nm/s
Kinetic solubility in PBS pH 7.4	421 μM
Basic pK_a (calculated, Percepta)	3.2
TPSA	129

[a]The screening cascade of assays implemented in our project ran aforementioned ADME stability measurements in human (h) and rat (r) versions in parallel, being rat the preclinical species selected for *in vivo* PK studies.

[b]Compounds were incubated with liver microsomes at 0.5 μM for 30 min.

[c]Compounds were incubated with hepatocytes at 0.5 μM for 180 min.

[d]Assay carried out in the presence of P-gp inhibitor elacridar.

The pharmacokinetic profile of compound **7** was evaluated in male CD rats following inhaled administration of a 0.5 mg/kg dose formulated as suspension, with a volume of administration of 0.5 mL/kg through intratracheal (*i.t.*) instillation (protocol detailed in Experimental Part). *i.t.* administration allows to deliver the compound solely to respiratory tract, thus reducing the risk of drug spill-over and absorption in the digestive tract, a fact that would alter tissue levels of the compound and hamper the precise understanding of drug disposition in the lung. Promising lung restriction of compound **7** was observed (Figure 6), with pulmonary levels 24–fold higher than plasma levels at the time when maximum lung concentration (C_{max}) was measured (T_{max} = 5

min). A sub-optimal lung half-life of 2.1 h, with no detectable drug in the lungs after 6 h following administration (T_{last} = 6 h), was conversely observed, this not being supportive of targeted once daily or twice daily administration of the drug.

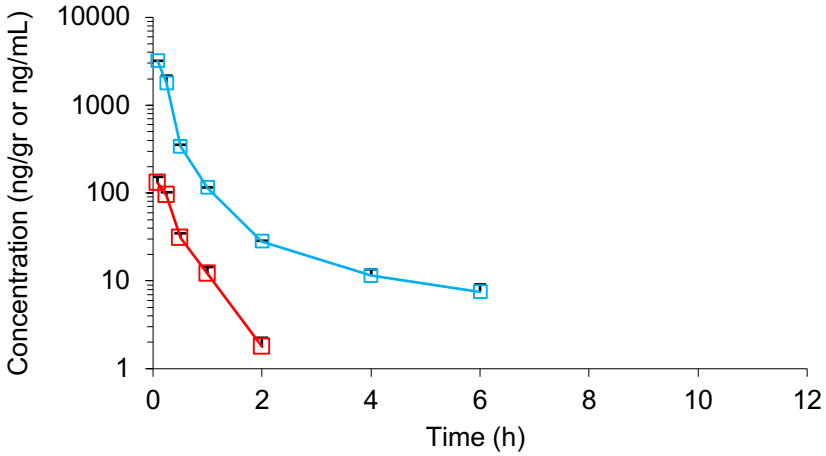

Figure 6. Lung (blue) and plasma (red) total concentrations and PK parameters after *i.t.* administration of compound **7** at 0.5 mg/kg in rat.

In vitro ADME/PhysChem profile of compound **7** was therefore reviewed in order to pinpoint prospected most sensible properties to be modulated in order to extend drug half-life in the lungs following *i.t.* administration. Optimal half-life in *in vitro* lung S9 assay was achieved of compound **7**. Additionally, while tuning compound solubility and dissolution rate has been reported as a strategy to increase residency in the respiratory tract,[33] clinical evidence has shown that reducing drug solubility in the lungs comes at the price of reducing the fraction of drug available to exert bioactivity, thus leading to a disconnect between drug levels in the lungs and pharmacodynamic effect (PK-PD disconnect).[34] In virtue of this, we decided not to purposely target low solubility of compounds in our drug discovery program. Intrinsic permeability

therefore emerged as the privileged property to be fine-tuned in order to maximise lung half-life of our inhaled PI3Kδ inhibitors.[33,35]

Lead Optimization: Lowering Permeability to Extend Lung Half-life.

Considering newly designed isocoumarin scaffold and *propeller-shape* conformation ensured the desired PI3Kδ selectivity, and that hinge binder and *affinity group* optimization led to low nanomolar potency in cell-based assay, permeability modulation was addressed by scoping chemical diversity at yet unoptimized head group portions of ligands (red colored in Figure 7). The design strategy involved the insertion of polar groups, and in most cases basic groups, as decorations of phenyl head group in either *para* (orange sub-series in Figure 7) or *meta* position (yellow sub-series in Figure 7) with respect to head group bond to isocoumarin scaffold. Additionally, novel, more flexible partially saturated heterocyclic head groups were explored, such as tetrahydropyridyn-3-yl head group (green sub-series in Figure 7) and tetrahydropyridyn-4-yl head group (blue sub-series in Figure 7). The use of basic functions is a well reported strategy to extend lung retention,[33] and it has been specifically applied to the design of inhaled PI3Kδ inhibitors.[36] Understanding the insertion of strongly basic groups would dramatically impact PhysChem and ADME properties, we decided to explore each head group sub-series in combination with two *affinity groups* of markedly different polarity (gray moieties in Figure 7), namely 3-hydroxypyridine *affinity group* of compound **7** and less polar 3-fluorophenol *affinity group* of comparatively potent and selective compound **6** (Figure 3, Table 4), in order to fine tune compound polarity at will.

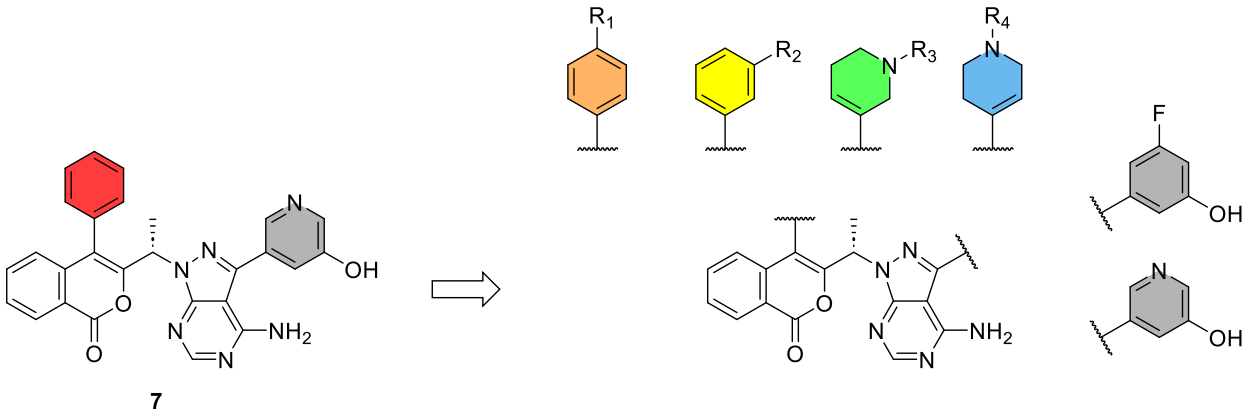

Figure 7. Regions of compound **7** selected for permeability optimization (head group, red; affinity group, gray) and representative head groups explored (orange, yellow, green, blue).

Meta and *para* topologies were comparatively analyzed in view of the decoration of phenyl and tetrahydropyridyl head groups, with initial assumptions later substantiated by X-ray crystallographic and docking data (Figure 8). In particular, *meta* topology was predicted to orient decorations toward an accessible, solvent exposed portion of the binding pocket (compound **9**, Figure 8b and Table 5), thus leading to favorable binding of ligands irrespective of head group nature. Conversely, different effect of *para* substitutions was predicted, depending on head group: flexibility of partially saturated tetrahydropyridyl ring was thought to allow binding even when bearing substituents in *p*-position with respect to link to scaffold (compound **10**, Figure 8c and Table 5). On the contrary, *para* substitutions on phenyl head group of compound **11** (Figure 8d) were expected to grow towards a sterically hindered region of the ATP-binding cleft, which could accommodate a restricted set of small head group substituents.

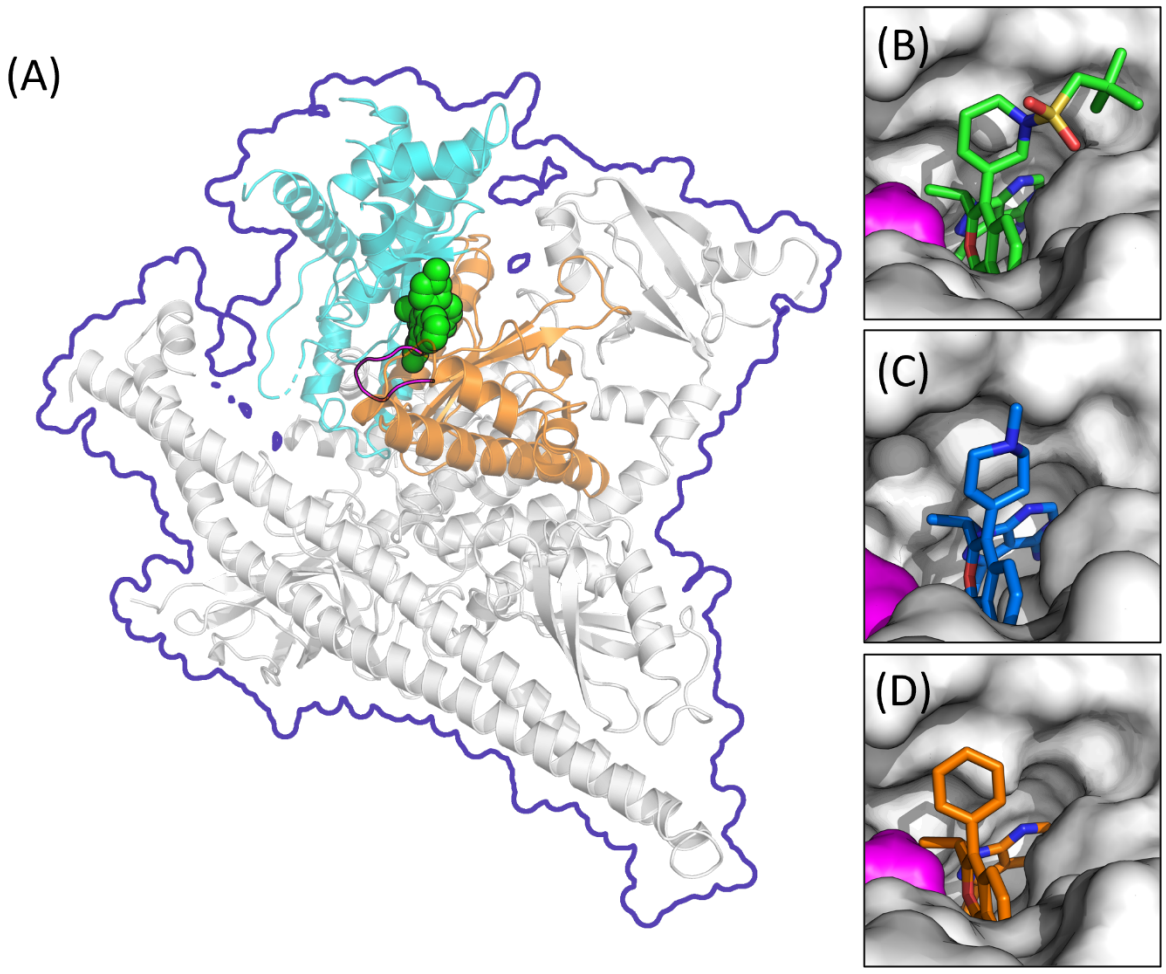

Figure 8. a) Comprehensive overview of the X-ray complex structure of compound **10** (green spheres) bound to hPI3Kδ (PDB code 9GDI). The N-lobe and the C-lobe of the kinase are colored in orange and cyan respectively. The p-loop segment is colored in magenta in all Figures 8a-d; b) docking of compound **9** (green carbons) into hPI3Kδ (PDB code 6G6W); c) X-ray crystal structure of compound **10** (blue carbons) bound to hPI3Kδ (PDB code 9GDI); d) superposition of the X-ray pose of compound **11** (orange carbons) within hPI3Kγ (PDB code 9GG9) and hPI3Kδ (PDB code 6G6W).

Comparison of representative matched pairs provided compelling evidence of divergent synergies between head group type (aromatic *vs* partially saturated) and substituent exit vector

topology (*para vs meta*). Compound **12**, displaying a *para*-decorated phenyl head group, resulted about 5-fold less potent in both enzymatic and cellular PI3Kδ assays than its *meta*-decorated analogue **13** (Table 5), again demonstrating that ligands embedding extended rigid moieties experience detrimental clashes with outer region of the binding pocket. In an opposite fashion, tetrahydropyridine head group led to equipotent compounds **14** and **15** despite their different exit vector topology, this reinstating the key role of flexible sp^3-rich head groups in allowing favorable binding to PI3Kδ.

Table 5. *In vitro* Pharmacology and Permeability Data of Head Group Sub-series Matched Pairs.

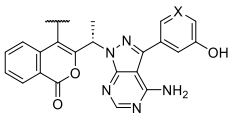

Compound	Head group	PI3Kδ pK_i[a]	PI3Kγ pK_i[a]	PI3Kβ pK_i[a]	PI3Kα pK_i[a]	THP-1 pIC_{50}[a]	Intrinsic permeability P_{app} AB[b]	TPSA
9	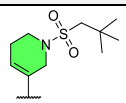 X = CF	8.65 ± 0.01	7.61 ± 0.03	6.24 ± 0.08	6.67 ± 0.11	8.51 ± 0.06	3.8 nm/s	154
10	 X = CF	9.13 ± 0.09	6.90 ± 0.09	8.09 ± 0.18	6.79 ± 0.04	8.97 ± 0.34	47 nm/s	119
11	 X = CF	9.12 ± 0.08	7.62 ± 0.02	6.74 ± 0.11	6.17 ± 0.01	8.26 ± 0.38	22 nm/s	116
12 (racemate)	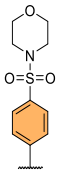 X = N	8.64 ± 0.07	7.29 ± 0.08	6.32 ± 0.12	6.63 ± 0.13	6.59 ± 0.29	n.t.[c]	176
13 (racemate)	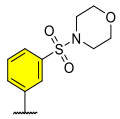 X = N	9.32 ± 0.09	7.46 ± 0.05	7.20 ± 0.02	6.45 ± 0.03	7.36 ± 0.14	2.4 nm/s	176

14	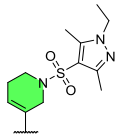 X = CF	8.64 ± 0.08	7.22 ± 0.05	5.78 ± 0.01	6.00 ± 0.03	8.44 ± 0.03	16.6 nm/s	171
15	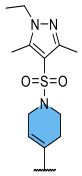 X = CF	8.74 ± 0.04	7.26 ± 0.04	6.30 ± 0.05	6.40 ± 0.11	8.46 ± 0.06	3.6 nm/s	171

[a]Data expressed as mean ± standard deviation of two independent determinations each in duplicate.

[b]Assay carried out in the presence of P-gp inhibitor elacridar.

[c]Compound not tested.

Further to detailed comparative analysis discussed above, aggregated analysis clearly showed that *meta* topology proved superior to *para* topology in providing PI3Kδ inhibitors of suitable potency in cell-based assay (green dots in Figure 9a and 9b *versus* Figure 9c and 9d respectively). Moreover, PI3Kδ selective ligands were obtained in all four head group sub-series across a range of substituents (dots in upper-right, green areas of graphs in Figure 9), thus underscoring the versatility of newly designed isocoumarin scaffold. Conversely, it was challenging to specifically correlate subtle modulations of selectivity with point structural differences in R substituents of head groups. As stated above, such substituents protrude in a solvent exposed area of the binding pocket, where any contact with PI3K surface is expected to be transient in nature, due to competing interaction of ligand with water molecules in the solvation shell. Therefore, rationalization of selectivity data would require elaborate analysis considering water networks, as previously reported by Robinson et al.[37]

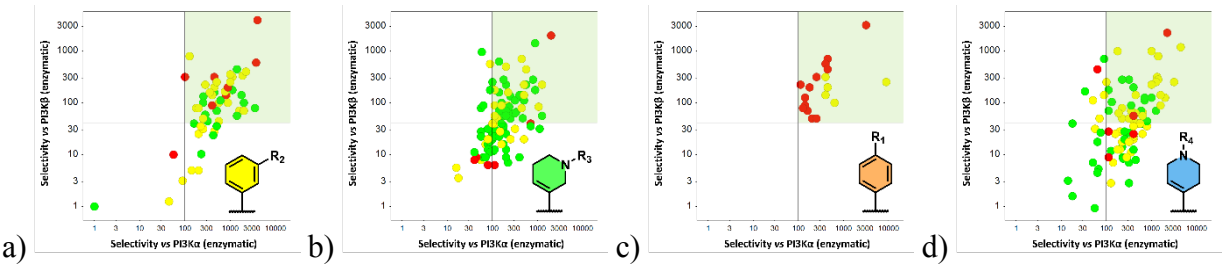

Figure 9. Enzymatic PI3Kδ/β fold selectivity *versus* PI3Kδ/α fold selectivity. Color coding according to cellular potency: pIC_{50} <7.5, red dots; 7.5< pIC_{50} <8.5, yellow dots; pIC_{50} >8.5, green dots; a) *m*-Ph head group sub-series; b) tetrahydropyridin-3-yl head group sub-series (*meta* topology); c) *p*-Ph head group sub-series; d) tetrahydropyridine-4-yl head group sub-series (*para* topology).

Having confirmed that diversity of decorated head groups was tolerated in terms of PI3Kδ potency and selectivity, newly designed compounds were tested in Caco-2 permeability assay to assess whether they indeed displayed desired lower permeability than compound **7**. Insertion of polar or basic moieties onto **7** expectedly drove TPSA to higher values, consequently lowering intrinsic permeability of tested lead compounds (Figure 10a, green box in upper-left part of graph). In this context, optimized hit compound **7** proved to be an advantageous starting point for permeability optimization, due to its high topological polar surface area (TPSA), already in the range of TPSA of inhaled PI3Kδ inhibitor GSK2292767 progressed to clinical trials and much higher than that of Idelalisib's (Figure 10b).

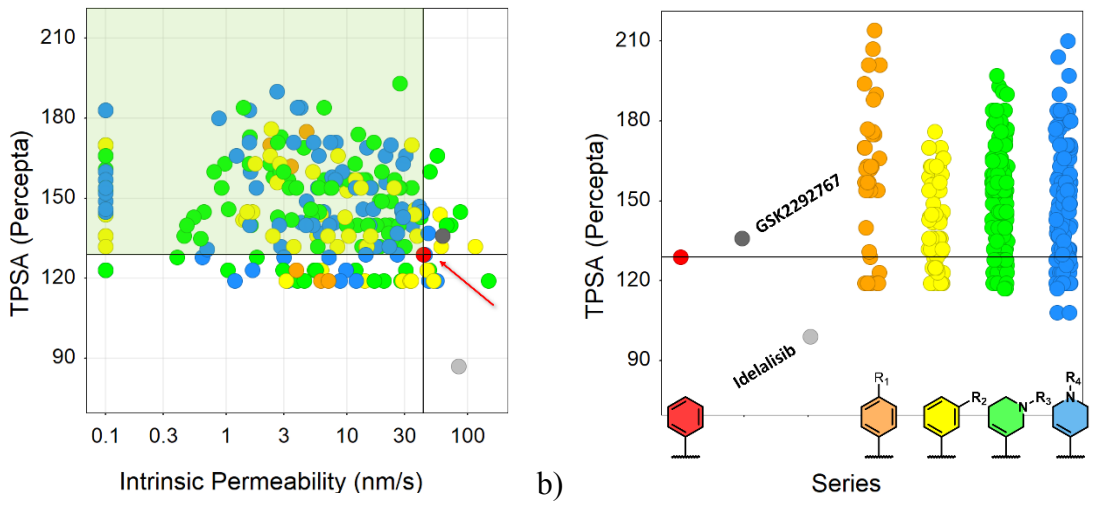

Figure 10. a) TPSA *versus* intrinsic permeability of lead compounds scoping diverse head groups. b) TPSA of lead compounds in comparison with TPSAs of compound **7** (red dot), GSK2292767 and Idelalisib.

In particular, insertion of *N*,*N*-dimethylaminomethyl group in *meta* position of compound **7** led to compound **16**, displaying much reduced permeability (3.6 nm/s *vs* 43 nm/s, Table 6), though proving suboptimal enzymatic selectivity with respect to PI3Kβ. Replacement of 3-hydroxypyridine *affinity group* of **16** with 3-fluorophenol yielded compound **17**, for which desired PI3Kδ/β selectivity was restored. However, a less polar *affinity group* caused a reduction in TPSA and consequent increase of intrinsic permeability to 14 nm/s. An alternative approach to rescue selectivity with respect to PI3Kβ involved the retention of 3-hydroxypyridine *affinity group* of **16** and the replacement of its *N*,*N*-dimethylamino decoration with a 1-methylpyperazinyl group, thus obtaining compound **18**: such compound matched low permeability of compound **16** with desired PI3Kδ selectivity. In an attempt to rationalize beneficial effect of 1-methylpyperazinyl decoration in reducing PI3Kβ pK_i of compound **18** with respect to compound **16** (1 log unit difference, Table 6), X-ray crystal structure of compound **18**

in complex with hPI3Kδ was solved. Interestingly, it was observed that 1-methylpyperazinyl group of compound **18** (cyan carbons, Figure 11a) protruded in a solvent exposed region of the binding pocket, highly accessible thanks to small, non-charged neighboring Thr-750 residue (magenta carbons, Figure 11a). Such residue is replaced by a bulkier, charged lysine residue in PI3Kβ (magenta carbons, Figure 11b), whereby electrostatic repulsion and steric hindrance with 1-methylpyperazinyl group could disfavor binding of compound **18** to PI3Kβ in comparison to compound **16**, featuring a smaller dimethylamino group instead. Nonetheless, since considered residues of PI3Kδ and β are in a solvent exposed, outer region of the binding pocket, any interaction with decorations of the ligands should be considered transient in nature, and effect of water network should be carefully considered.[37]

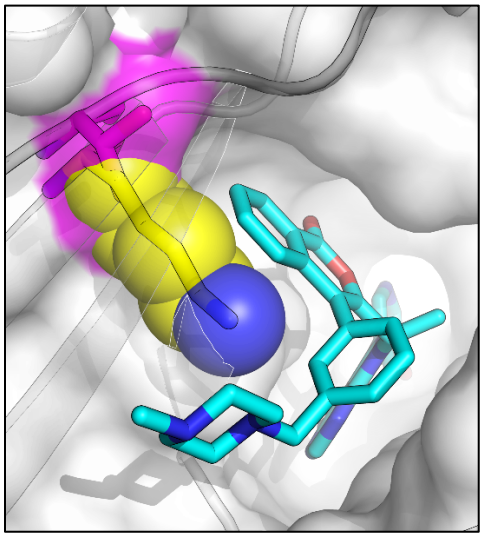

Figure 11. Superposition of the X-ray crystal structure of compound **18** (cyan carbons) in complex with hPI3Kδ (white cartoon, magenta carbons and surface for Thr-750, PDB code 9GCF) to murine PI3Kβ (yellow carbons for Lys-771, PDB code 4BFR; this lysine is conserved in hPI3Kβ).

Replacement of phenyl head group of compound **7** with tetrahydropyridin-3-yl head group of compound **19** resulted in a PI3Kδ potent and selective compound of much reduced permeability (Table 6). In this case, since the two compounds displayed same values of TPSA, the reduction of permeability was likely due to the insertion of a basic group in the ligand and to the addition of a H-bond donor. Nonetheless, removal of such H-bond donor and decrease of basic center pK_a by *N*-alkylation of compound **19** led to compound **20**, which still displayed reduced permeability with respect to compound **7** and an overall appealing PI3Kδ inhibitory profile. Moreover, compounds in the tetrahydropyridin-3-yl head group sub-series featuring two basic centers, such as compounds **21** and **22**, or no basic centers, such as compound **23**, were designed, in order to elucidate whether the number of basic centers[36] would impact lung retention beyond the effect of intrinsic permeability of compounds. As a matter of fact, all three compounds **21**, **22** and **23** displayed permeability values comparable to each other and only slightly reduced with respect to compound **7**. Additionally, head group of compound **23** was further elaborated in order to restore the presence of a basic moiety, which **23** did not display. Therefore, compound **24** was designed and prepared: pleasingly, its intrinsic permeability was dramatically reduced with respect to compound **23**. In tetrahydropyridin-4-yl sub-series, compound **25** (Table 6) displayed a dramatically reduced permeability with respect to compound **7**, similarly to its tetrahydropyridin-3-yl regioisomer **19**. However, compound **25** resulted an equipotent inhibitor of PI3Kδ and PI3Kβ in enzymatic assay, thus completely losing its selectivity with respect to the latter isoform. Alkylation of nitrogen atom of the tetrahydropyridinyl ring as in compound **26**, or conversion of the amino group into corresponding sulfonamide as in compound **27**, allowed to rescue PI3Kδ selectivity while reducing intrinsic permeability in comparison to compound **7**.

Table 6. *In vitro* Pharmacology and Permeability Data of Compounds Exploring Diverse Head Groups.

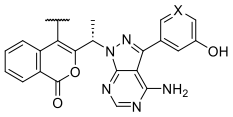

Compound	Head group	PI3Kδ pK_i[a]	PI3Kγ pK_i[a]	PI3Kβ pK_i[a]	PI3Kα pK_i[a]	THP-1 pIC_{50}[a]	Intrinsic permeability P_{app} AB[b]	TPSA	Basic pK_a[c]
7	 X = N	9.2 ± 0.10	8.1 ± 0.16	7.5 ± 0.07	6.7 ± 0.03	8.8 ± 0.22	43 nm/s	129	3.2
16	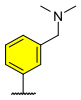 X = N	9.28 ± 0.00	7.72 ± 0.00	8.24 ± 0.08	6.99 ± 0.03	9.2 ± 0.05	3.6 nm/s	132	8.7
17	 X = CF	9.46 ± 0.00	6.51 ± 0.04	7.24 ± 0.05	6.47 ± 0.04	8.81 ± 0.00	14 nm/s	119	8.7
18 (CHF-6523)	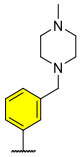 X = N	9.07 ± 0.02	7.05 ± 0.03	7.26 ± 0.05	6.66 ± 0.01	8.78 ± 0.06	5.6 nm/s	136	7.6
19	 X = CF	9.18 ± 0.04	6.04 ± 0.15	7.64 ± 0.11	6.18 ± 0.09	8.95 ± 0.31	1.8 nm/s	128	9.1
20	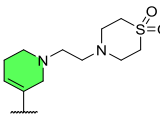 X = CF	9.51 ± 0.02	7.86 ± 0.02	7.74 ± 0.01	6.77 ± 0.10	8.77 ± 0.34	9.4 nm/s	157	7.2
21	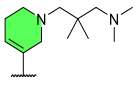 X = CF	9.44 ± 0.03	7.62 ± 0.06	7.09 ± 0.03	7.16 ± 0.03	8.98 ± 0.07	12 nm/s	123	9.6 6.6
22	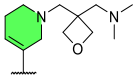 X = CF	9.21 ± 0.03	7.47 ± 0.05	7.50 ± 0.03	6.81 ± 0.10	9.38[d]	19 nm/s	132	9.1 5.8
23	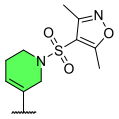	9.63 ± 0.06	8.39 ± 0.05	7.43 ± 0.06	6.91 ± 0.04	9.42 ± 0.08	28 nm/s	193	3.2

	X = N								
24	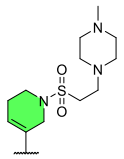	9.13 ± 0.10	6.74 ± 0.09	6.68 ± 0.01	6.89 ± 0.03	8.53 ± 0.14	0.8 nm/s	160	7.6
	X = CF								
25		8.23 ± 0.09	6.60 ± 0.07	8.33 ± 0.09	6.53 ± 0.06	9.13 ± 0.18	0.6 nm/s	128	9.4
	X = CF								
26	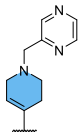	9.00 ± 0.02	6.74 ± 0.04	6.94 ± 0.04	5.92 ± 0.06	9.06 ± 0.01	29 nm/s	145	6.7
	X = CF								
27	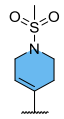	9.49 ± 0.18	8.04 ± 0.06	7.44 ± 0.03	7.44 ± 0.01	8.78 ± 0.03	5.7 nm/s	154	3.6
	X = CF								

[a]Data expressed as mean ± standard deviation of two independent determinations each in duplicate.

[b]Assay carried out in the presence of P-gp inhibitor elacridar.

[c]Calculated pK_a of main basic centers (Percepta).

[d]n = 1.

Compounds **17-24**, **26** and **27** in the sub-series discussed above, which displayed desired PI3Kδ selectivity and potency, together with reduced intrinsic permeability with respect to compound **7**, were progressed to *in vivo* pharmacokinetic studies (Figure 12a). Pleasingly, markedly higher levels in lungs and notably extended lung retentions with respect to compound **7** were observed (Table 7, red plot in Figure 12a), with compounds still detected in the lungs at 24 h post administration. In particular, 20– to 630–fold improvements in lung $AUC_{0\text{-last}}$ were registered, with at least doubled pulmonary half life, apart for compounds **24** and **26**, which therefore were not considered for progression to *in vivo* pharmacodynamic studies. In particular, compound **24** displayed the shortest lung half-life among compounds progressed to *i.t.* PK, possibly as a

consequence of its lower metabolic stability in rat lung S9 fraction with respect to other compounds (Table 7 and green plot in Figure 12a). Remarkably, compounds **21** and **22**, which embedded two basic centers, did not show significantly higher lung AUCs or longer lung half-lives with respect to compounds with similar intrinsic permeability bearing only one (compound **17**) or no basic centers (compound **23**). On the contrary, compounds **21** and **22** were found to redistribute from plasma to heart, and were consequently discontinued because of the risk of undesired side effects.

Table 7. *In vivo* PK Data of Compounds Administered to Rats by Intratracheal Instillation at 0.5 mg/kg dose.

Compound	Lung S9 $t_{1/2}$ h, r	Lung $AUC_{0\text{-last, total}}$ h*ng/g	Lung $t_{1/2}$ h	Lung-plasma split at Lung T_{max} = 5 min	Heart-plasma split at Lung T_{max} = 5 min
7	>146 min[a], >146 min[a]	979	2.09	24	n.t.[a]
17	>146 min[a], >146 min[a]	21400	4.79	152	n.t.
18 (CHF-6523)	>514 min, >514 min	42300	4.94	189	1.0
19	>514 min, >514 min	258000	5.56	3406	n.t.
20	n.t., n.t.	79800	7.03	621	1.6
21	344 min, 299 min	32400	4.78	125	4.7
22	334 min, 324 min	11400	5.62	142	4.1
23	>514 min, >514 min	92400	10.8	142	0.35
24	>514 min, 240 min	20600	0.68	513	2.2
26	>514 min, >514 min	180000	2.94	734	1.0
27	>514 min, >514 min	623000	n.d.[b]	21288	n.t.

[a]Compound not tested.

[a]Flat lung PK profile did not allow to calculate lung half-life.

Increased lung half life of *i.t.* administered compounds supported our working hypothesis of reducing intrinsic permeability of compounds to extend lung retention (Figure 12b).

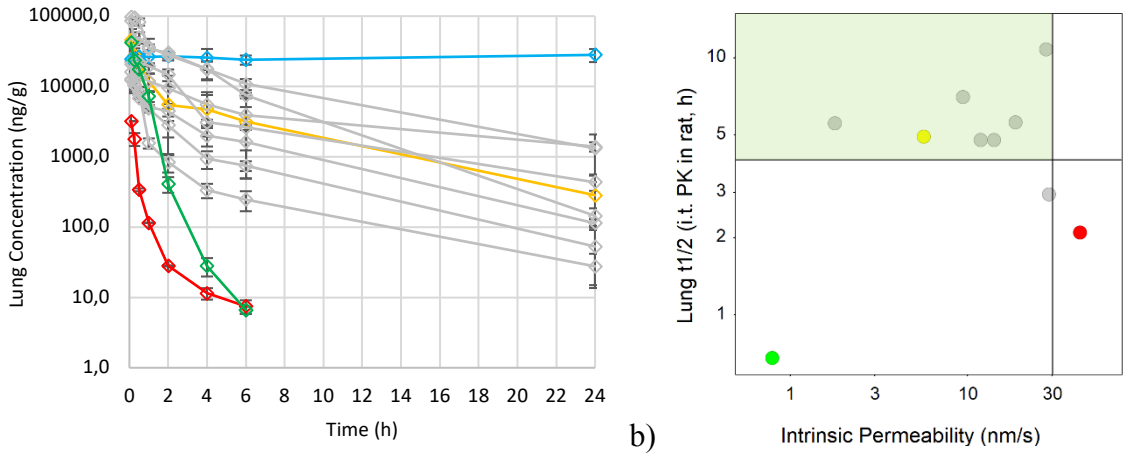

Figure 12. a) Lung total concentrations after *i.t.* administration of compounds at 0.5 mg/kg in rat b) Lung half-lives *versus* intrinsic permeability. Compound **7**, red; compound **24**, green; compound **27**, blue; compound **18**, yellow; compounds **17**, **19-23**, **26**: gray; (flat lung PK profile of compound **27** did not allow to calculate lung half-life, missing dot in Figure 12b).

Late Lead Optimization: *In Vivo* Efficacy of Compounds.

Lead compounds **17-20**, **23** and **27**, which displayed the best lung PK profiles, were selected for testing in ovalbumin (OVA) *in vivo* pharmacodynamic model of airway inflammation, in order to establish whether adequate exposure in lung of *in vitro* potent compounds would translate into efficacy in an *in vivo* setting. Doses tested in OVA PD model (0.1 and 1.0 μmol/kg) were selected prospecting human doses that could be administered by inhalation devices (up to ~1 mg/administration), while timepoints were defined in order to first highlight compound efficacy (-2 h), and then amenability to twice daily administration (-12 h) (protocols fully detailed in Experimental Part).

Table 8. *In vivo* Pharmacodynamic Data in Ovalbumin Model of Airway Inflammation and Selected ADME/PhysChem Data.

Compound	**17**	**18** (CHF-6523)	**19**	**20**	**23**	**27**
BALF Eosinophils (-2 h, 0.1 μmol/kg)	0[a]	-78%	-68%	-66%	0[a]	0[a]
BALF Eosinophils (-2 h, 1.0 μmol/kg)	-65%	-96%	-86%	-70%	0[a]	0[a]
BALF Eosinophils (-12 h, 0.1 μmol/kg)	n.t.[b]	-55%	0[a]	-49%	n.t.	n.t.
BALF Eosinophils (-12 h, 1.0 μmol/kg)	n.t.	-67%	0[a]	-91%	n.t.	n.t.
Kinetic solubility in PBS pH 7.4	402 μM	441 μM	410 μM	312 μM	50 μM	BQL[c]
Lung free fraction (rat)	1.9%	3.3%	1.2%	3.0%	1.1%	1.4%

[a]No statistically significant modulation of eosinophil count in BALF.

[b]Compound not tested

[c]Below quantitation limit

Compounds **18**, **19** and **20** modulated eosinophilia also at lower 0.1 μmol/kg administered dose (Table 8), hence were progressed to the duration of action (DoA) protocol, involving compound administration 12 h before *i.t.* OVA instillation. Gratifyingly, compounds **18** and **20** downregulated eosinophil recruitment in the lungs at both tested doses also in DoA PD protocol, thus emerging as PI3Kδ selective inhibitors, characterised by long lung retention following topical administration in the respiratory tract, and showing persistent pharmacodynamic effect in the lungs. The latter compounds were therefore subjected to the exploration and identification of solid forms amenable to administration as inhaled dry powder.

Envisaging Administration as Dry Powder: Salt and Polymorph Screening.

Intended administration of identified PI3Kδ inhibitors *on top* of COPD therapies combining inhaled corticosteroids with bronchodilators, prompted the quest of solid forms of compounds **18** and **20** that could be administered through dry powder inhalers (DPIs), alone or in combination with the other therapeutic agents. Salt screening and polymorph screening for the two

compounds therefore ensued. A suitable form of crystalline mono-maleate salt of **18** and of the anhydrous crystalline free base of compound **20** and were identified through salt and polymorph screening studies. We then proceeded to a comparison of lung and plasma profiles of identified forms of mono-maleate salt of **18** (Figure 13a) and of anhydrous free base of **20** (Figure 13b), by administration either as a wet formulation or as a dry powder, with the purpose of demonstrating that identified forms were suitable for administration by inhalation. Pleasingly, PK profiles of the two formulations were superimposable for each of the two compounds, with lung half-lives in suitable range for delivery of dry powders by inhalation (13.1 h for compound **18** mono-maleate dry powder, 9.7 h for compound **20** anhydrous free base dry powder).

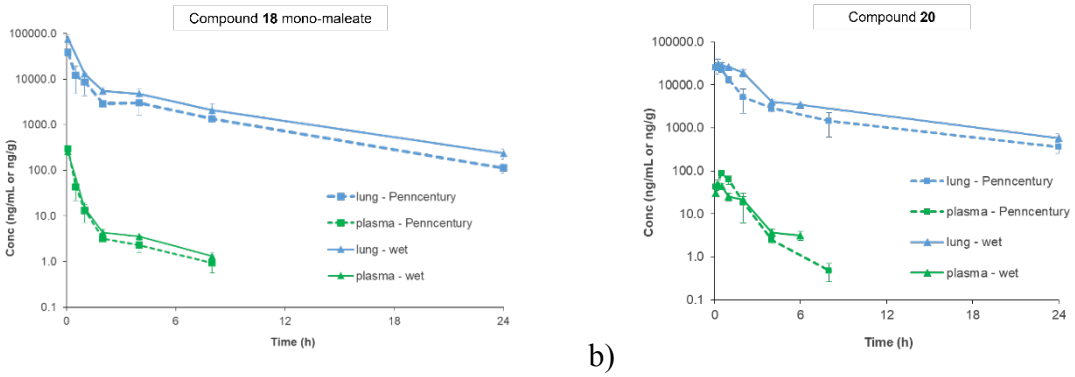

a) b)

Figure 13. a) Lung (blue plots) and plasma (green plots) total concentrations of compound **18** mono-maleate at 0.5 mg/kg in rat: *i.t.* administration of wet formulation (solid line), DP administered through PennCentury insufflator (dashed lines). b) Lung (blue plots) and plasma (green plots) total concentrations of compound **20** anhydrous free base at 0.5 mg/kg in rat: *i.t.* administration of wet formulation (solid lines), DP administered through PennCentury insufflator (dashed lines).

Finally, efficacy of identified dry powders of the two compounds was again assessed in OVA PD model, in order to rule out any PK-PD disconnect brought about by a change in dissolution rates, and to highlight any difference in efficacy between selected solid forms of the two compounds.

While dry powders of both PI3Kδ inhibitors confirmed their ability in downregulating eosinophil recruitment in BALF when administered 2 h before inflammatory trigger, only dry powder of mono-maleate of compound **18** displayed persistent efficacy in DoA protocol involving drug administration 12 h before ovalbumin *i.t.* instillation (Figure 14a).

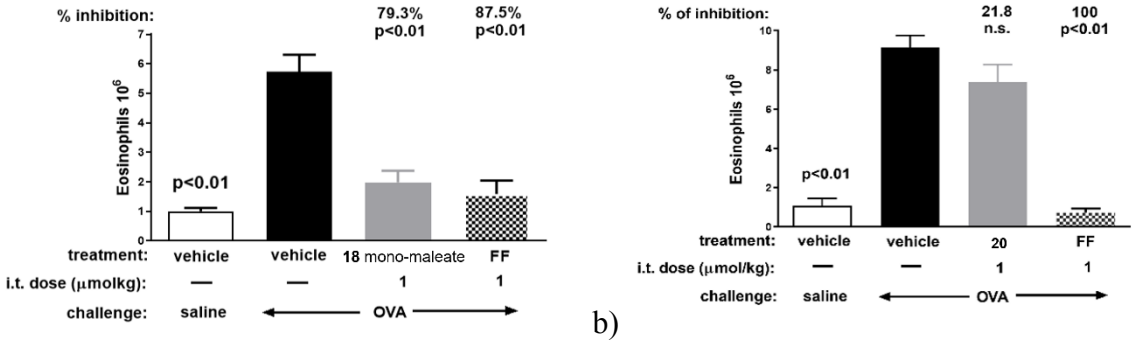

Figure 14. *In vivo* OVA PD data of compounds **18** mono-maleate and **20** administered as dry powders in DoA protocol (compounds administered 12 h before pro-inflammatory trigger), with fluticasone furoate (FF) used as a positive control. a) compound **18** mono-maleate; b) compound **20**.

Eventually, the design and preparation of more than 900 compounds in the newly discovered isocoumarin series achieved the optimization of PI3Kδ selectivity, cellular potency, intrinsic permeability and lung retention. Following solid state studies and final confirmation of *in vivo* PK and efficacy culminated in the identification of mono-maleate of compound **18** as a derivative with an overall appealing profile (Table 9). Therefore, compound **18** mono-maleate was nominated as clinical candidate CHF-6523 and was advanced to detailed safety and toxicological characterization in view of progression to clinical studies.

Table 9. *In vitro* Pharmacology, ADME, PhysChem Properties and *In Vivo* PK and PD Data of CHF-6523 (**18**).

Property	Value

PI3Kδ enzymatic pK_i[a]	9.07 ± 0.02
PI3Kγ pK_i[a]	7.05 ± 0.03
PI3Kβ pK_i[a]	7.26 ± 0.05
PI3Kα pK_i[a]	6.66 ± 0.01
THP-1 cellular pIC_{50}[a]	8.78 ± 0.06
Lung S9 $t_{1/2}$	>514 min (h) – >514 min (r)[b]
Hepatic Microsomes $t_{1/2}$[c]	128 min (h) – 121 min (r)
Hepatocytes $t_{1/2}$[d]	193 min (h) – 33 min (r)
Intrinsic permeability (Caco-2 $P_{app}AB$[e])	5.6 nm/s
Kinetic solubility in PBS pH 7.4	441 μM
Lung $AUC_{0\text{-last, total}}$ (DP, PennCentury, 0.5 mg/kg)	47735 h*ng/g
Lung $t_{1/2}$ (DP, PennCentury, 0.5 mg/kg)	13.1 h
Lung-plasma split (at Lung T_{max} = 5 min)	129
BALF Eosinophils (DP, -2 h, 1.0 μmol/kg)	-64.8%
BALF Eosinophils (DP, -12 h, 1.0 μmol/kg)	-79.3%

[a]Data expressed as mean ± standard deviation of two independent determinations each in duplicate.

[b]The screening cascade of assays implemented in our project ran aforementioned ADME stability measurements in human (h) and rat (r) versions in parallel, being rat the preclinical species selected for *in vivo* PK studies.

[c]Compounds were incubated with liver microsomes at 0.5 μM for 30 min.

[d]Compounds were incubated with hepatocytes at 0.5 μM for 180 min.

[e]Assay carried out in the presence of P-gp inhibitor elacridar.

Safety and Toxicology Characterization.

Besides generally pursuing safety of newly designed compounds by optimizing selectivity toward PI3Kα and β, and by targeting lung restriction and minimal systemic exposure, specific further characterizations were devoted to rule out unintended pharmacological activity or toxic properties of compound CHF-6523 (**18**). The target selectivity of CHF-6523 (**18**) was profiled against 468 human kinases, using the scanMAX Kinase Profiling Panel (Eurofins Discovery). At the test concentration of 1 μM (corresponding to 100% inhibition of PI3Kδ), only two additional kinases showed an inhibition greater than 90%: PI3Kβ (96%) and PI3Kγ (90%), both belonging to the same enzyme class (Figure 15, see Supporting Information for full details).

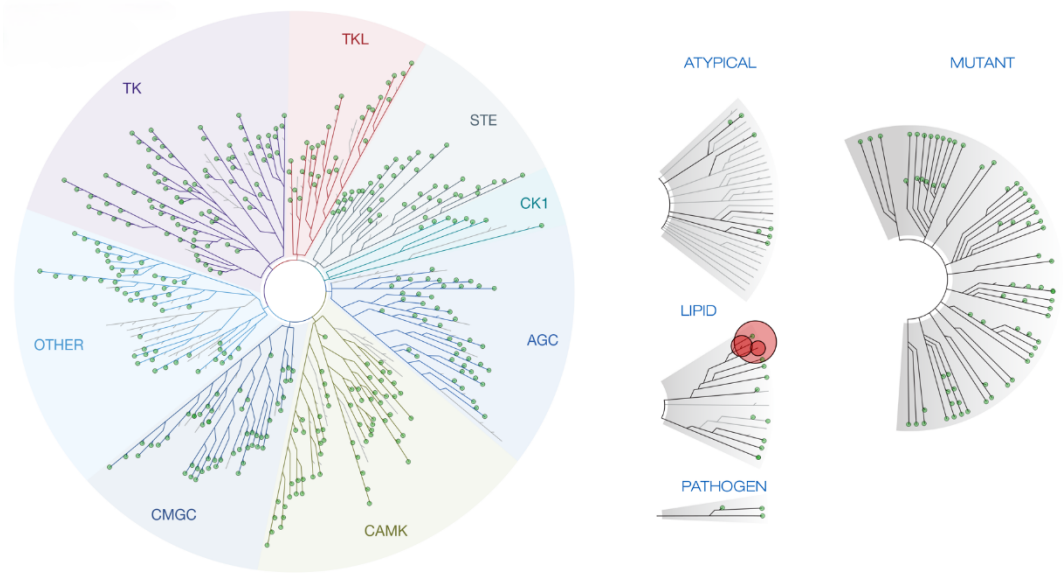

Figure 15. Selectivity of CHF-6523 (**18**) in the human kinome. TREE*spot* depicting the selectivity of CHF-6523 (**18**) screened against 468 kinases via the scanMAX Kinase Profiling Panel (Eurofins Discovery) at 1 μM. Red dots identify hits PI3Kδ, PI3Kβ and PI3Kγ.

Selectivity of CHF-6523 (**18**) was also evaluated in the LeadProfilingScreen panel of 68 assays (Eurofins Discovery), comprising receptors, ion channels, enzymes and transporters involved in a variety of biological processes and potentially linked to unwanted effects. At a concentration of 1 μM, CHF-6523 (**18**) did not show significant interactions with any of the target in the panel. Similarly, CHF-6523 (**18**) displayed no inhibition of CYP450 recombinant enzymes 1A2, 2B6, 2C8, 2C9, 2C19, 2D6 and 3A4 (>50 μM IC_{50}s), and it was not converted into unique metabolites following incubation in the presence of human hepatocytes. The compound showed a clean profile in the non-GLP assays aimed to detect mutagenic potential (Ames test) and cardiovascular liabilities (hERG assay and *in vivo* telemetry in dogs after single inhaled dose). Moreover, in the preliminary toxicity studies in rats and dogs, once daily inhaled administration of CHF-6523 (**18**) for 2 weeks was well tolerated *in vivo* up to high doses without any relevant

histology finding, indicating the potential for CHF-6523 (**18**) of achieving good safety margins in subsequent longer Toxicology studies. Negligible oral bioavailability of CHF-6523 (**18**) was measured in *in vivo* PK studies in rat (unpublished data), thus ruling out side effects arising from gastrointestinal absorption of swallowed fraction of drug administered by inhalation. Finally, the compound progressed to good laboratory practice (GLP) safety pharmacology and toxicology studies to support the PhI Clinical study. The candidate showed no mutagenic, clastogenic or aneugenic potential and the Safety Pharmacology studies identified no risks on the central nervous, respiratory or cardiovascular systems (hERG NOEL>100 μM in GLP assay). In repeat dose Toxicology studies of 4 weeks in rats and dogs, the no observed adverse effect levels (NOAELs) allowed to calculate adequate safety margins over a predicted 1.8 mg/day therapeutic human dose, based on either deposited lungs dose (rat: 200-fold, dog: 150-fold, based on mean body/lungs weights at the NOAELs at the end of treatment, 10% lungs deposition of the achieved dose in rats and 25% in dogs, 100% lungs deposition in man and man lungs' weight of 1000 g) or on predicted systemic exposure (rat: 4 to 8-fold, dog: 34 to 43-fold, based on mean $AUC_{0\text{-}24}$ values in preclinical species at the NOAELs on days 1 and 28 and a predicted human $AUC_{0\text{-}24}$ of 33.8 ng*h/mL based on PBPK modelling calculations).

Synthetic Chemistry. Compounds **1**, **2**, **3**, **4**, **5**, **6**, **7**, **8**, **11**, **17**, and intermediates **28**, **32**, **36a** were synthesized as described in WO 2015/091685. Compound **10** was obtained by chiral chromatographic separation of corresponding racemic mixture, whose preparation is reported in WO 2015/091685. Compound **16** was synthesized as described in WO 2020/200918. Compounds **12** and **13** were prepared starting from intermediate **28** and following the synthetic sequence reported in Scheme 1: Suzuki cross-coupling installed head groups R_1 to give

intermediates **29**, which were converted into corresponding alkyl bromides **30**, then subject to nucleophilic substitution to give aryl iodides **31**. Final Suzuki cross-coupling installed *affinity group* to yield compounds **12** and **13**.

Scheme 1. Synthesis of compounds **12** and **13**[a]

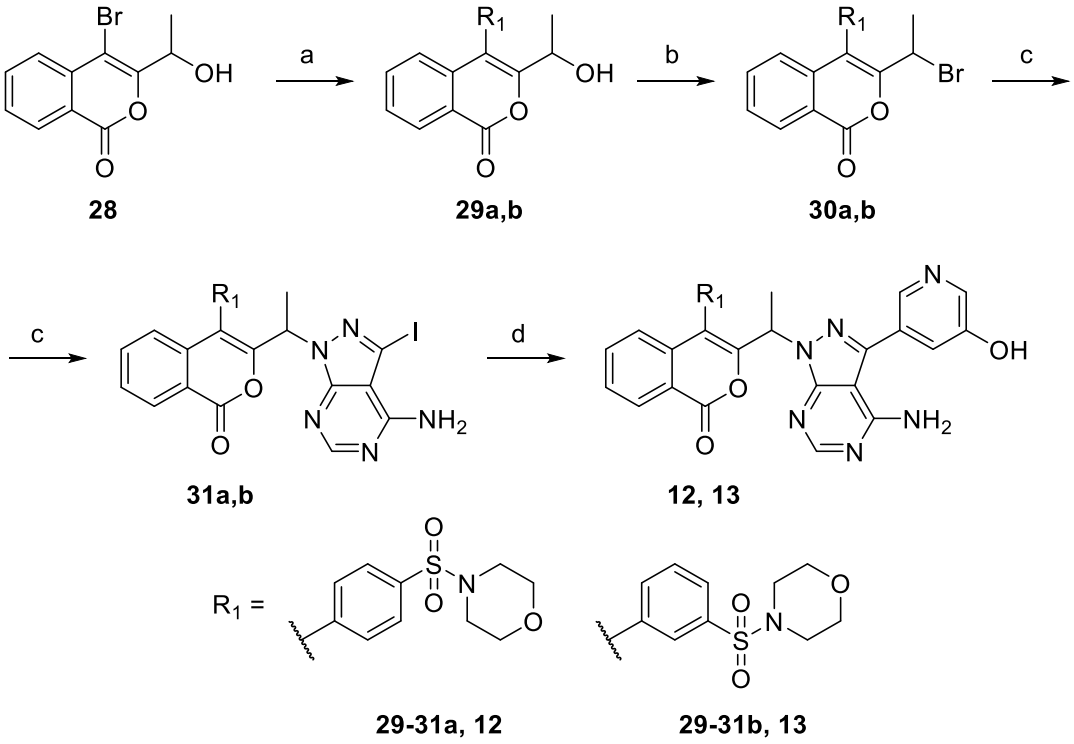

[a](a) Boronic acid or ester, K_3PO_4, XPhos Pd(crotyl)Cl, THF/H_2O 1:1, 50 ºC; (b) PBr_3, DCM, 0 ºC; r.t.; (c) BBr_3, DCM, r.t.; (d) boronic ester, K_3PO_4, SPhos Pd G2, THF/H_2O 3:1, MW 80 ºC.

Enantiopure compounds in tetrahydropyridin-3-yl head group sub-series were prepared starting from optically pure intermediate **34**, which was prepared according to Scheme 2, starting from corresponding intermediate **32**, through chiral chromatography yielding single enantiomer **33** and subsequent cleavage of Boc protecting group. Alternatively, intermediate **33** was subject to Suzuki cross-coupling, followed by acidic treatment, to directly yield compound **19**.

Scheme 2. Synthesis of intermediate **34** and compound **19**[a]

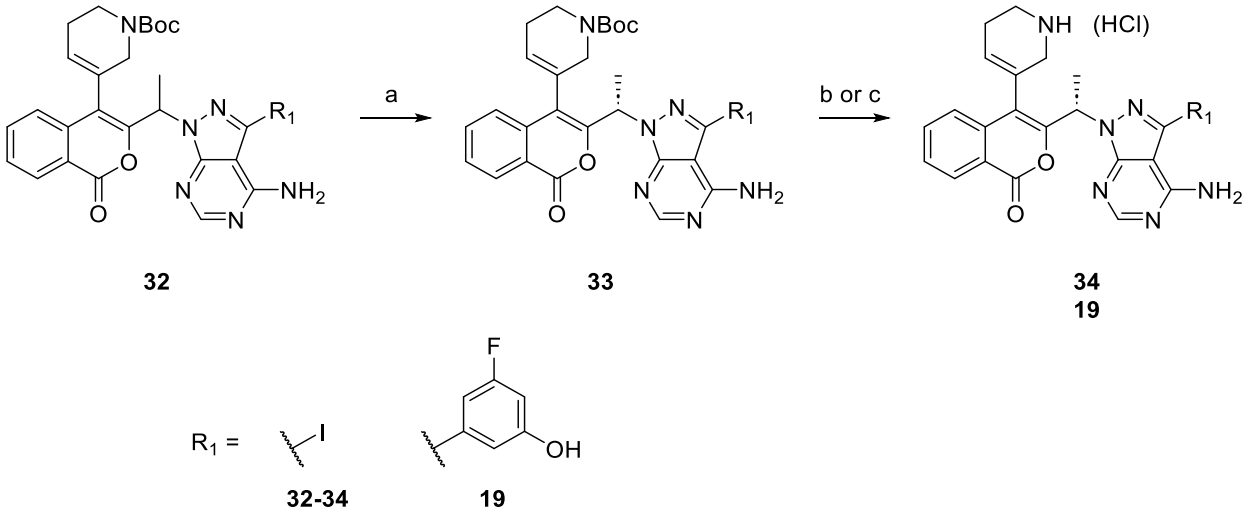

[a](a) Preparative chiral chromatography; (b) 1.25 M HCl, MeOH, r.t.; (c) boronic acid, K_3PO_4, SPhos Pd G2, THF/H_2O 3:1, MW 80 ºC, then 4.0 M HCl, 1,4-dioxane, r.t.

Compounds **9**, **14**, **20**, **21**, **23**, and **24** were prepared according to Scheme 3 starting from intermediate **34**. Substituents R_1 were introduced by either direct *N*-sulfonylation (yielding intermediates **35a**, **b**, **e**) or *N*-alkylation of tetrahydropyridinyl ring (yielding intermediate **35c**), or by reductive amination (yielding intermediate **35d**). In the case of compound **24**, a two step procedure involving first *N*-vinylsulfonylation and then β-addition of 1-methylpiperazine yielded intermediate **35f**. Subsequently, *affinity groups* were installed on intermediates **35** through Suzuki cross-coupling reactions yielding final compounds **9**, **14**, **20**, **21**, **23** and **24**.

Scheme 3. Synthesis of compounds **9**, **14**, **20**, **21**, **23** and **24**[a]

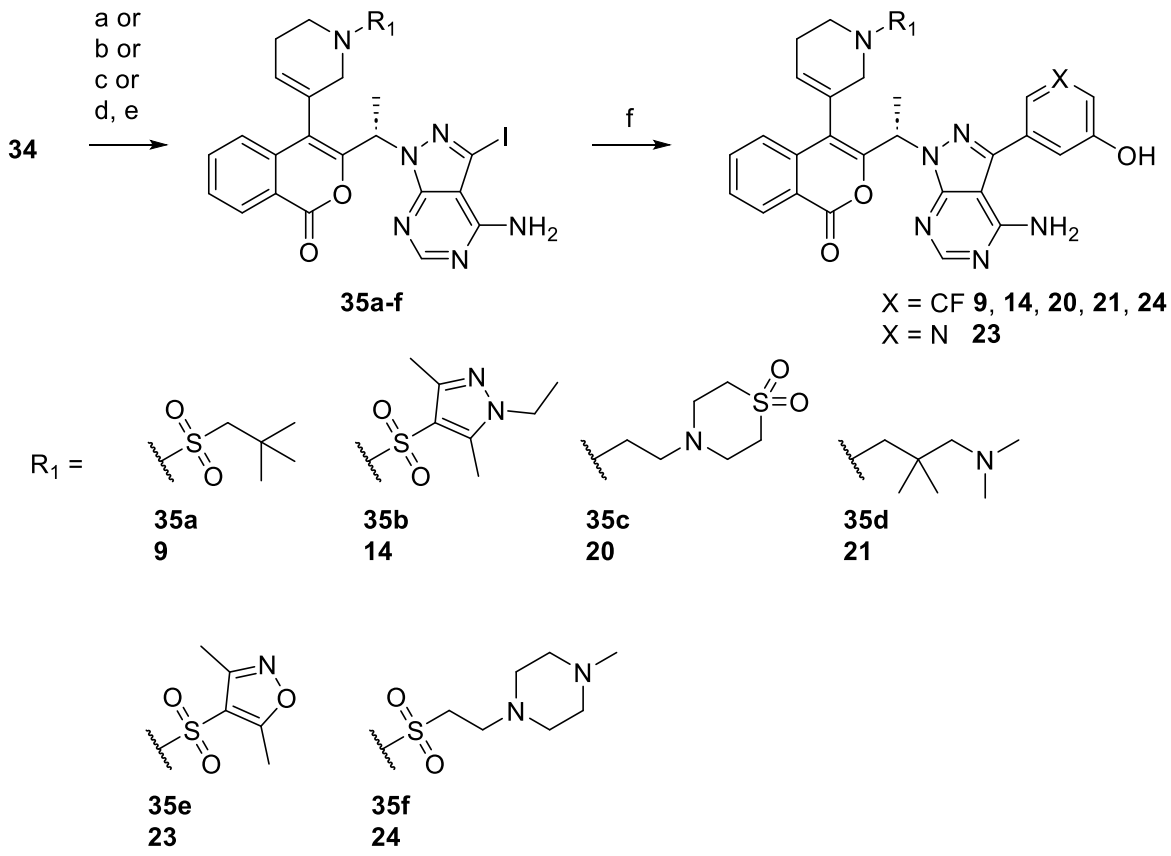

[a](a) Sulfonylchloride, NEt_3, DCM, 0 ºC; (b) alkyl halide, KI, K_2CO_3, DMF, r.t.; (c) aldehyde, $Na(OAc)_3BH$, AcOH, DIPEA, DCM, r.t.; (d) 2-chloroethanesulfonyl chloride, TEA, DMAP, DMF, r.t.; (e) *N*-methyl piperazine, THF, r.t.; (f) boronic acid or ester, K_3PO_4, SPhos Pd G2, THF/H_2O 3:1, MW 80 ºC.

Enantiopure compounds in tetrahydropyridin-4-yl head group sub-series were prepared starting from optically pure intermediate **38a**, which was prepared starting from corresponding intermediate **36a** through chiral chromatography yielding single enantiomer **37a**, and subsequent cleavage of Boc protecting group (Scheme 4). Alternatively, intermediate **36a** was converted into intermediate **36b** by means of a Suzuki-cross coupling reaction. Chiral chromatograpy purification of compound **36b** followed to yield enantiopure intermediate **37b**. Subsequent simultaneous cleavage of *N*-Boc and *O*-methyl protecting groups of compound **37b** directly yielded compound **25**.

Scheme 4. Synthesis of intermediate **38a** and compound **25**[a]

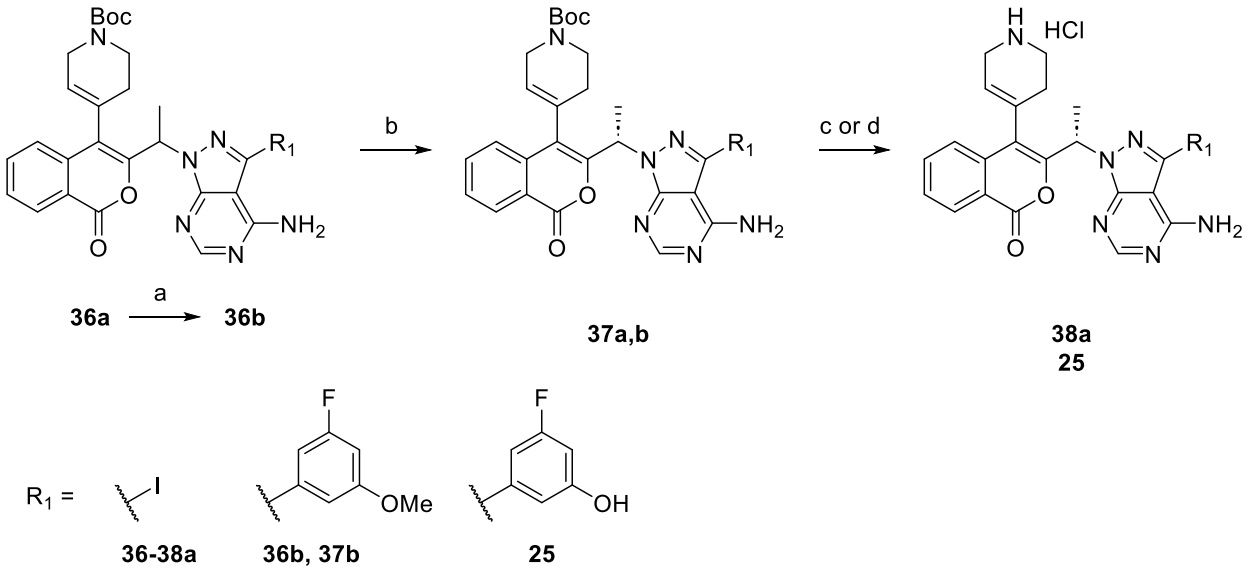

[a](a) Boronic acid, K_2CO_3, Pd(dppf)Cl_2, 1,4-dioxane, 110 ºC; (b) preparative chiral chromatography; (c) 1.25 M HCl, MeOH, r.t.; (d) BBr_3, DCM, 0 ºC.

Compounds **15**, **26** and **27** were prepared either by *N*-sulfonylation or by reductive amination of intermediate **38a** to give intermediates **39**, from which Suzuki cross-coupling reactions yielded final compounds (Scheme 5).

Scheme 5. Synthesis of compounds **15**, **26** and **27**[a]

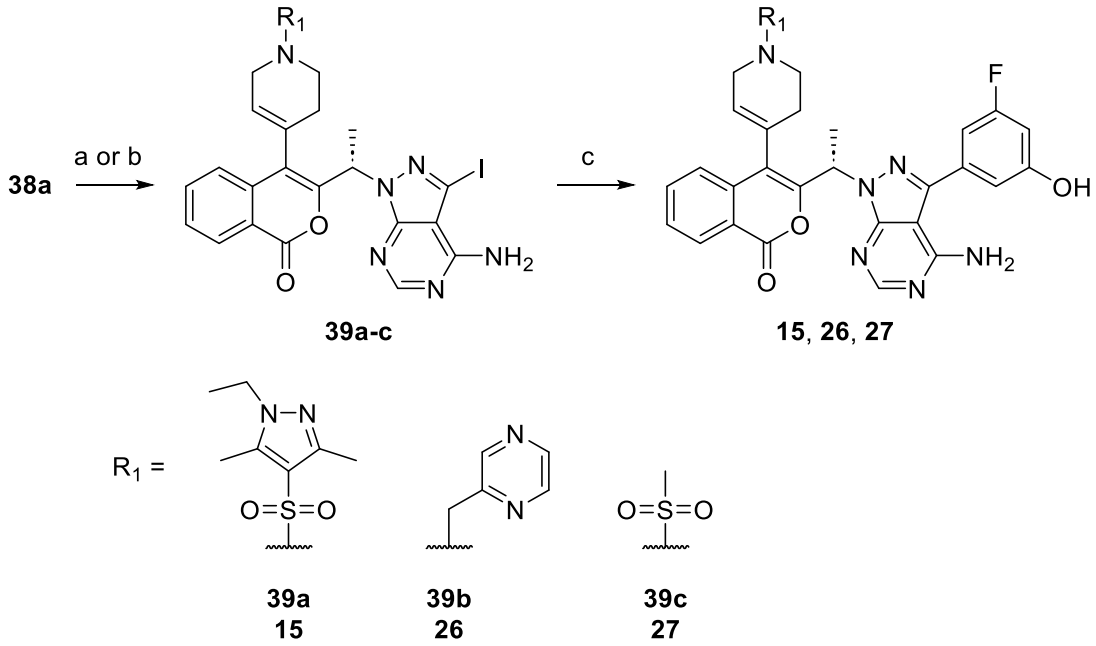

[a](a) Sulfonylchloride, NEt_3, DCM, 0 ºC; (b) aldehyde, $Na(OAc)_3BH$, AcOH, DIPEA, DCM, r.t.; (c) boronic acid, K_3PO_4, SPhos Pd G2, THF/H_2O 3:1, MW 80 ºC.

Alkyl group on tetrahydropyridin-3-yl head group of compound **22** was constructed started from intermediate **34** through a sequence of *N*-alkylation, alcohol **40** oxidation to aldehyde **41** and reductive amination reactions to yield intermediate **42** (Scheme 6). Suzuki cross-coupling followed and yielded final compound **22**.

Scheme 6. Synthesis of compound **22**[a]

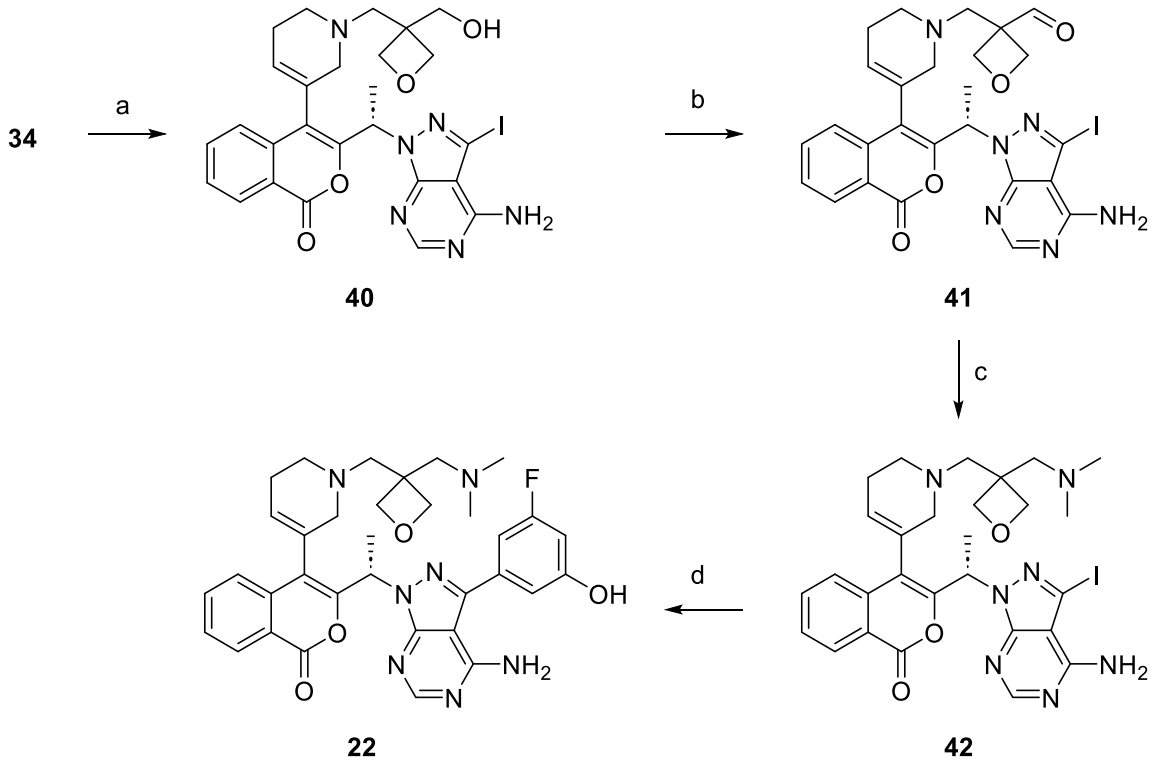

[a](a) alkyl bromide, KI, K_2CO_3, acetone, rt; (b) Dess-Martin periodinane, DCM, r.t.; (c) aldehyde, $Na(OAc)_3BH$, AcOH, DIPEA, DCM, r.t.; (d) boronic acid, K_3PO_4, SPhos Pd G2, THF/H_2O 3:1, MW 80 ºC.

Compound **18** (CHF-6523) was prepared as reported in WO 2020/200918 and summarized in Scheme 7. Intermediate **44** was prepared starting from compound **28** by means of Suzuki cross-coupling yielding compound **43** and subsequent aldehyde deprotection. Reductive amination then yielded compound **45**, whose hydroxyl group was converted into alkyl bromide group of compound **46**. Nucleophilic substitution followed to install hinge binder with protected affinity

group, thus yielding intermediate **47**. Finally, acidic deprotection of affinity group afforded intermediate **48** and preparative chiral HPLC led to the isolation of compound **18** (CHF-6523).

Scheme 7. Synthesis of compound CHF-6523 (**18**)[a]

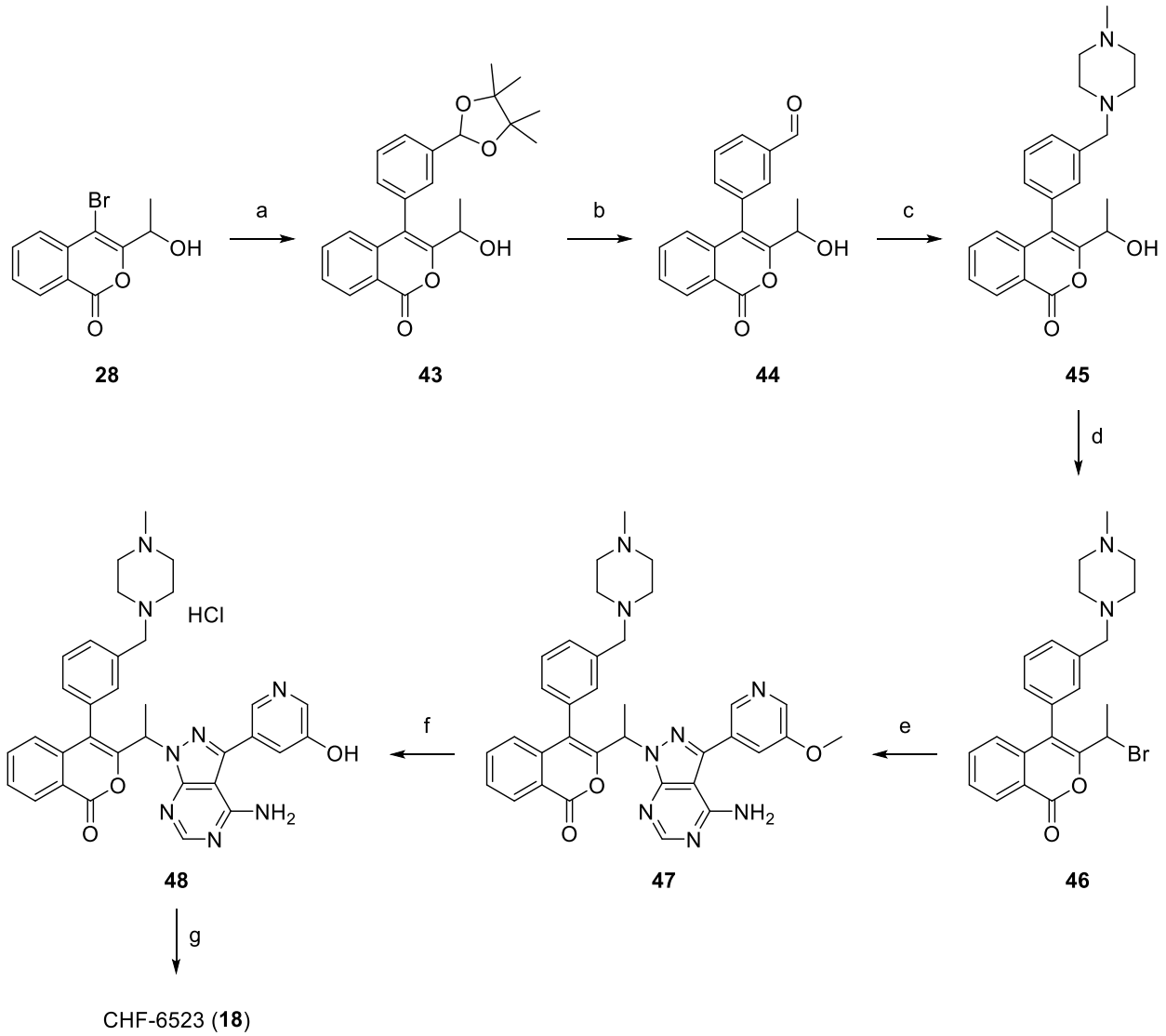

[a](a) boronate ester, XPhos Pd G2, $K_3PO_4 \cdot H_2O$, THF/water 1:1, r.t.; (b) 1 M HCl, MeCN, r.t.; (c) 1-methylpiperazine, $NaBH(AcO)_3$, AcOH, DCM, r.t.; (d) PBr_3, DCM, r.t.; (e) 3-(5-methoxypyridin-3-yl)-1*H*-pyrazolo[3,4-*d*]pyrimidin-4-amine, K_2CO_3, DMF, r.t. to 40 ºC; (f) BBr_3, DCM, r.t.; (g) preparative chiral HPLC.

Conclusions.

Our resolution to provide novel therapeutic options to exacerbating COPD patients prompted a drug discovery campaign pursuing the identification of selective PI3Kδ inhibitors to be administered by inhalation. Strategic choice of propeller-shaped ligands and the design of the novel isocoumarin series scaffold were successful in consistently providing desired selectivity with respect to PI3Kα and β. Cellular potency suitable for compound delivery by the inhalatory route was reached by hinge binder and *affinity group* optimization. Intrinsic permeability optimization was elected as fruitful strategy to achieve high drug levels in the lungs and long pulmonary half-lives following administration by inhalation. Compounds **18** and **20**, matching high PI3Kδ potency and selectivity, desired lung pharmacokinetic profiles, and durable downregulation of lung inflammatory infiltrate in a relevant *in vivo* pharmacodynamic model, were identified. A crystalline form of mono-maleate of compound **18**, suitable for DPI formulation, was identified and it confirmed desired inhalational pharmacokinetic profile, as well as sustained anti-inflammatory efficacy *in vivo*. Compound **18** mono-maleate was thus identified as clinical candidate CHF-6523, whose excellent *in vitro* safety profile and behavior in Safety Pharmacology and GLP Toxicology studies eventually confirmed suitability for *first-in-human* dosing. CHF-6523 (**18**) was indeed progressed to clinical studies in healthy volunteers and COPD patients. Safety, tolerability and efficacy outcomes of clinical trials were recently disclosed.[38]

EXPERIMENTAL PART

***In vitro* Pharmacology: PI3Kδ, -γ, -β, -α ADP-Glo™ assay, THP-1 Cellular Assay.** See Bruno et al.[27]

***In vitro* Pharmacology: Human Kinome Selectivity.** Compound **18** (CHF-6523) was tested at 1 μM in the scanMAX KINOMEscan® profiling panel, comprising binding assays for 468 human kinases. Experimental conditions for each assay are available at the provider's website (https://www.eurofinsdiscovery.com/catalog/scanmax-kinase-kinomescan-leadhunter-panel-us/87-0001-1000). Images were generated using TREEspot™ Software Tool and reprinted with permission from KINOMEscan®, a division of DiscoveRx Corporation, © DISCOVERX CORPORATION 2010.

***In vitro* Pharmacology: LeadProfilingScreen Safety Panel.** Compound **18** (CHF-6523) was tested in the LeadProfilingScreen panel provided by Eurofins Discovery. This panel consists of 68 different enzyme and radioligand binding assays to help identify potential off-targets. The conditions for each assay can be found at the provider's website (https://www.eurofinsdiscovery.com/catalog/leadprofilingscreen-safetyscreen-panel-tw/PP68).

PhysChem: Kinetic Solubility in PBS pH 7.4. See Mazzucato et al.[28]

***In vitro* ADME: Metabolic Stability in Lung S9 Fraction, Caco-2 Membrane Permeability Assay.** See Bruno et al.[27] **Lung Tissue Binding Measurement.** See Mazzucato et al.[28]

***In vivo* Studies.** Animal studies were approved by the Chiesi Farmaceutici S.p.A. Ethical Committee and conducted in accordance with the local legislation and institutional requirements. Specifically, the experimental procedures involving animals were approved by Italian Ministry of Health and complied with the European Directive 2010/63 UE and Italian D.Lgs 26/2014 for

animal care and use of laboratory animals. and were carried out with efforts to minimize the number of animals used and their suffering.

***In vivo* Studies: Intratracheal Pharmacokinetic Protocol A (Figures 6 and 12a, solid lines in Figures 13a and 13b).** Intratracheal administration procedure was carried out as described previously (Bruno et al.[27]), setting the following time points: 0.083, 0.25, 0.5, 1, 2, 4, 6 and 24 h post dose for liquid formulations. Heart was sampled at four timepoints (0.25, 2, 6 and 24 h post dose).

***In vivo* Studies: Intratracheal Pharmacokinetic Study Protocol B (dashed lines in Figures 13a and 13b).** Protocol B differs from Protocol A for the following details. A PennCentury DP4 insufflator (Penncentury Inc., PA, USA) was used for the intratracheal delivery of the compounds as dry powder (DP). Before dosing, the insufflator was loaded with a weighed amount of the DP formulation and connected through a valve to a plastic syringe whose plunger was equipped with a spring that is necessary for the propulsion for powder delivery. The steel termination of the PennCentury device was inserted in the catheter placed in the animal trachea, similarly to the procedure followed for the administration of liquid formulations. After administration, plasma and lung were collected at the following time points: 0.083, 0.5, 1, 2, 4, 8 and 24 h.

***In vivo* Studies: OVA Inflammation Model.** *Animals.* Male Brown Norway rats (6 weeks old at the arrival) were purchased from Charles River Laboratories Italy (Calco, Lecco). Prior to studies, animals were acclimated for at least 5 days to the local vivarium conditions (room temperature: 20-24 °C; relative humidity: 40-70%), having free access to standard rat chow and tap water.

Sensitization and allergen exposure. Animals were sensitized by intraperitoneal injection of a suspension containing OVA (1 mg/rat) and $Al(OH)_3$ (100 mg/rat) in 1 mL of saline for 3 consecutive days. Two/three weeks later, the airway inflammation was induced by inhaled antigen. The animals were exposed to an aerosol of OVA solution (1% in saline) that induced a massive influx of inflammatory cells, mainly eosinophils and neutrophils, into the airways. Briefly, rats were restrained in plexiglass tubes and exposed to the content of the inhalation chamber by nose-only inhalation for 30 min. The inhalation chamber was connected to a Medel Pro nebulizer that generated aerosolized ovalbumin that circulated through the chamber at the flow rate of approximately 3.3 L/min. The vehicle-control treated animals were exposed to aerosolized saline.

Treatment with test compounds. For the assessment of inhibitory potency, test compounds were administered by the intratracheal route 2 or 12 hours before OVA challenge. For the intratracheal administration of test compounds or vehicle, animals were anaesthetized with sevoflurane (4% in oxygen) and a laryngoscope was moved forward into the mouth to visualize the trachea and guide the insertion of a PE100 cannula or a PennCentury directly into the trachea and located 1-2 mm above the bifurcation for solution or DP respectively. Test compounds administered as dry powder were micronized and blended with 0.2% w/w magnesium stearate/Respitose SV003 7.75% strengths for the dose of 1 μmol/kg with an injection weight of 10 mg/kg. Control animals received 10 mg/kg of blend. The compound suspensions or DP were blown into the airways during the spontaneous phase inspiration in an air volume of 2 mL or 4ml respectively.

Bronchoalveolar lavage and cell counting. At 24 after exposure either to OVA or saline aerosol, animals were anaesthetised with isoflurane or sevoflurane as previously described and sacrificed by bleeding from the abdominal aorta. Bronchoalveolar lavage fluid (BALF) was obtained by

gently washing the lungs with 3 aliquots (4 mL each) of solution A [Hank's balanced salt solution (HBSS) × 10, 100 mL; ethylenediaminetetraacetic acid (EDTA) 100 mM, 100 mL; 4-(2-hydroxy-ethyl)-1-piperazineethansulphonic acid (HEPES) 1 mM, 10 mL; distilled water, 790 mL]. Routine recovery of BALF did not significantly differ between animals with ~80% of instilled volume recovered (9.5-10.5 mL). The resulting BALF was centrifuged at 800 × *g* for 10 min at 4° C. The pellets deriving from the same animal were combined and resuspended in a volume of 1.5 mL and total and differential cell counts were performed within 2 hours using an automated cell counter (Dasit, Sysmex). The cell count per animal was calculated from the number of cells for 1 µL of BALF multiplied for the volume used for the re-suspension of the cell pellet.

Data analysis. All data are presented as mean ± standard deviation. Statistical analysis was performed on raw data using one-way analysis of variance (ANOVA) followed by Dunnett's *post-hoc* test for comparison with the OVA-sensitised, OVA-challenged group. The drug-induced *individual* changes were calculated comparing the drug-treated with the vehicle-treated OVA challenged control animals.

$$effect = 100 \times \frac{(Treated - Challenged) - (Challenged - Sham)}{(Challenged - Sham)}$$

Treated = drug-treated OVA challenged *individual* value

Challenged = mean OVA-challenged control

Sham = mean sham-challenged control

Statistical analysis was performed using GraphPad software, version 7.0, $p<0.05$ was considered a level of statistical significance.

Chemistry: General Methods. All solvents and reagents were commercially available from common suppliers such as Fluorochem or Sigma Aldrich and were used as purchased without

further purification. Where the preparation of starting materials is not described, these are commercially available, known in the literature, or readily obtainable by those skilled in the art using standard procedures. ^{1}H-NMR spectra were recorded on a Varian MR-400 spectrometer operating at 400 MHZ (proton frequency), equipped with a self-shielded Z-gradient coil 5 mm 1H/nX broadband probe head for reverse detection, deuterium digital lock channel unit, quadrature digital detection unit with transmitter offset frequency shift, or on AgilentVNMRS-500 or on a Bruker Avance 400 spectrometers. Chemical shift are reported in parts per million using the residual nondeuterated solvent as the internal standard (for CDCl3: 7.26 ppm, ^{1}H; for DMSOd6: 2.50 ppm; for CD3OD: 3.34 ppm). Coupling constants (*J* values) are given in hertz (Hz) and multiplicities are reported using the following abbreviation (s = singlet, d = doublet, t = triplet, q = quartet, m = multiplet, br. = broad). Chiral QC methods, preparative reversed-phase high-performance liquid chromatography (HPLC) methods, and flash column chromatography description are detailed in the Supporting Information. The purity of all compounds screened in the biological assays was estimated by LC/UV/MS analysis and was found to be ≥95%.

Chemistry: Preparation of Compounds. *General Procedure A: Suzuki cross-coupling.* A mixture of aryl iodide (1 eq), boronic acid or ester (2-4 eq) and K_3PO_4 (3 eq) in THF/water (3:1) was deoxygenated by N_2 bubbling for 10 min, then SPhos Pd G2 (0.15 eq) was added and the mixture was heated at 80 °C under MW irradiation. The organic solvent was removed under reduced pressure and the residue was extracted with DCM (3×). Combined organic layers were washed with brine and dried over Na_2SO_4, then filtered and concentrated under reduced pressure. Crude mxiture was purified by column chromatography.

*(S)-3-(1-(4-amino-3-(3-fluoro-5-hydroxyphenyl)-1H-pyrazolo[3,4-d]pyrimidin-1-yl)ethyl)-4-(1-(neopentylsulfonyl)-1,2,5,6-tetrahydropyridin-3-yl)-1H-isochromen-1-one (**9**)*. The title

compound was synthesized according to the general procedure A, starting from (*S*)-3-(1-(4-amino-3-iodo-1*H*-pyrazolo[3,4-*d*]pyrimidin-1-yl)ethyl)-4-(1-(neopentylsulfonyl)-1,2,5,6-tetrahydropyridin-3-yl)-1*H*-isochromen-1-one (0.058 g, 0.089 mmol) and (3-fluoro-5-hydroxyphenyl)boronic acid (0.028 g, 0.178 mmol). Yield 53% (0.030 g, 0.047 mmol). UPLC−MS (method 11), rt 1.10 min, $[M+H]^+$ 633.2. ^{1}H NMR (400 MHz, DMSO-d_6) δ ppm 10.10-10.39 (m, 1H), 8.24-8.30 (m, 1H), 8.14-8.24 (m, 1H), 7.85-7.97 (m, 1H), 7.61-7.72 (m, 1H), 7.42-7.58 (m, 1H), 6.81-6.99 (m, 2H), 6.62-6.72 (m, 1H), 5.36-6.29 (m, 2H), 2.22-4.05 (m, 8H), 1.80-1.95 (m, 3H), 1.01-1.16 (m, 9H).

*(S)-3-(1-(4-amino-3-(3-fluoro-5-hydroxyphenyl)-1H-pyrazolo[3,4-d]pyrimidin-1-yl)ethyl)-4-(1-methyl-1,2,3,6-tetrahydropyridin-4-yl)-1H-isochromen-1-one (**10**).* Racemate 3-(1-(4-amino-3-(3-fluoro-5-hydroxyphenyl)-1H-pyrazolo[3,4-*d*]pyrimidin-1-yl)ethyl)-4-(1-methyl-1,2,3,6-tetrahydropyridin-4-yl)-1H-isochromen-1-one (0.320 g, 0.624 mmol) was dissolved in DMF (4.8 mL) and submitted to chiral resolution by Chiral preparative chromatography. Conditions: Column: Chiralpak IA (25 x 2.0 cm, 5 µm); Mobile phase: n-hexane/(2-propanol/methanol 1:1 + 0.1% isopropylamine) 73/27% v/v; Flow rate 16 mL/min; DAD detection: 280 nm; Loop: 150 µL; Injection: 10 mg/injection. The fractions containing the second eluted enantiomer were evaporated to dryness (0.115 g, 0.209 mmol). Further purification by reversed-phase liquid chromatography followed (12g Biotage C-18 cartridge, gradient elution from H_2O/acetonitrile 95:5 to H_2O/acetonitrile 70:30, with 0.1% HCOOH). Fractions were collected and prior to drying 2 mL of 1 M HCl were added. Concentration under reduced pressure afforded title compound (0.110 g, 0.200 mmol, 32% yield). Chiral HPLC (method A14), rt 7.4 min, e.e. >99%. UPLC−MS (method 11), rt 0.58 min, $[M+H]^+$ 513.3. ^{1}H NMR (400 MHz, DMSO-d_6) δ ppm 11.44 (s, 1H), 11.20 (s, 0H), 11.10 (s, 0H), 10.36 (s, 1H), 8.57 (s, 0H), 8.50 (s, 0H), 8.45 (s, 0H),

8.38 (s, 0H), 8.24 – 8.12 (m, 1H), 8.03 – 7.80 (m, 2H), 7.72 – 7.61 (m, 1H), 7.54 (dd, J = 10.6, 8.0 Hz, 0H), 7.02 – 6.83 (m, 2H), 6.74 (ddq, J = 10.1, 5.7, 2.1 Hz, 1H), 6.41 (q, J = 6.8 Hz, 0H), 6.32 (q, J = 7.0 Hz, 0H), 6.23 (q, J = 7.0 Hz, 0H), 6.17 – 6.03 (m, 1H), 5.51 (s, 0H), 4.03 (d, J = 16.9 Hz, 1H), 3.85 (dd, J = 18.4, 11.8 Hz, 1H), 3.52 (s, 0H), 3.39 (s, 1H), 3.00 – 2.88 (m, 4H), 2.79 (s, 0H), 2.58 (d, J = 18.3 Hz, 1H), 2.03 – 1.85 (m, 3H), 1.25 (s, 0H).

*3-(1-(4-amino-3-(5-hydroxypyridin-3-yl)-1H-pyrazolo[3,4-d]pyrimidin-1-yl)ethyl)-4-(4-(morpholinosulfonyl)phenyl)-1H-isochromen-1-one (**12**)*. The title compound was synthesized according to the general procedure A, starting from 3-(1-(4-amino-3-iodo-1*H*-pyrazolo[3,4-*d*]pyrimidin-1-yl)ethyl)-4-(4-(morpholinosulfonyl)phenyl)-1*H*-isochromen-1-one (0.294 g, 0.45 mmol) and 5-(4,4,5,5-tetramethyl-[1,3,2]dioxaborolan-2-yl)pyridin-3-ol (0.395 g, 1.78 mmol). Yield 11% (0.032 g, 0.05 mmol). UPLC−MS (method 9), rt 0.78 min, $[M+H]^+$ 626.5. ^{1}H-NMR (DMSO-d6, 400MHz): δ 8.29 - 8.24 (m, 2H), 8.19 (d, 1H), 8.09 (s, 1H), 7.92 (dd, 1H), 7.81–7.77 (m, 2H), 7.71 (dd, 1H), 7.65 (t, 1H), 7.34-7.38 (m, 2H), 6.89 (d, 1H), 5.74 (q, 1H), 3.70 (t, 4H), 2.90-3.00 (m, 4H), 1.84 (d, 3H).

*3-(1-(4-amino-3-(5-hydroxypyridin-3-yl)-1H-pyrazolo[3,4-d]pyrimidin-1-yl)ethyl)-4-(3-(morpholinosulfonyl)phenyl)-1H-isochromen-1-one (**13**)*. The title compound was synthesized according to the general procedure A, starting from 3-(1-(4-amino-3-iodo-1*H*-pyrazolo[3,4-*d*]pyrimidin-1-yl)ethyl)-4-(3-(morpholinosulfonyl)phenyl)-1*H*-isochromen-1-one (66.5 mg, 0.10 mmol) and 5-(4,4,5,5-tetramethyl-[1,3,2]dioxaborolan-2-yl)pyridin-3-ol (88.4 mg, 0.40 mmol). Yield 27% (16.7 mg, 0.027 mmol). UPLC−MS (method 9), rt 0.75 and 0.78 min (possible atropoisomers), $[M+H]^+$ 626.4. ^{1}H-NMR (DMSO-d6, 400MHz, mixture of diastereoisomers): δ 8.27-8.21 (m, 2H), 8.19 (t, 1H), 8.12-8.03 (m, 1H), 7.89-7.72 (m, 4H), 7.68-7.54 (m, 2H), 7.38-

7.26 (m, 1H), 6.89-6.81 (m, 1H), 5.84-5.60 (m, 1H), 3.68 (t, 4H), 3.61-3.47 (m, 1H), 3.10-2.93 (m, 1H), 2.87-2.77 (m, 2H), 1.91-1.79 (m, 3H).

*(S)-3-(1-(4-amino-3-(3-fluoro-5-hydroxyphenyl)-1H-pyrazolo[3,4-d]pyrimidin-1-yl)ethyl)-4-(1-((1-ethyl-3,5-dimethyl-1H-pyrazol-4-yl)sulfonyl)-1,2,5,6-tetrahydropyridin-3-yl)-1H-isochromen-1-one (**14**).* The title compound was synthesized according to the general procedure A, starting from (*S*)-3-(1-(4-amino-3-iodo-1*H*-pyrazolo[3,4-*d*]pyrimidin-1-yl)ethyl)-4-(1-((1-ethyl-3,5-dimethyl-1*H*-pyrazol-4-yl)sulfonyl)-1,2,5,6-tetrahydropyridin-3-yl)-1*H*-isochromen-1-one (0.099 g, 0.140 mmol) and (3-fluoro-5-hydroxyphenyl)boronic acid (0.044 g, 0.280 mmol). Yield 47% (0.045 g, 0.066 mmol). UPLC−MS (method 12), rt 0.92 min, $[M+H]^+$ 684.30. ^{1}H NMR (400 MHz, DMSO-d_6) δ ppm 9.82-10.64 (m, 1H), 8.09-8.31 (m, 1H), 7.80-7.99 (m, 2H), 7.57-7.75 (m, 1H), 7.36-7.47 (m, 1H), 6.78-6.98 (m, 2H), 6.58-6.73 (m, 1H), 5.30-6.24 (m, 2H), 3.95-4.14 (m, 2H), 2.87-3.80 (m, 6H), 2.11-2.45 (m, 6H), 1.74-1.91 (m, 3H), 1.21-1.37 (m, 3H).

*(S)-3-(1-(4-amino-3-(3-fluoro-5-hydroxyphenyl)-1H-pyrazolo[3,4-d]pyrimidin-1-yl)ethyl)-4-(1-((1-ethyl-3,5-dimethyl-1H-pyrazol-4-yl)sulfonyl)-1,2,3,6-tetrahydropyridin-4-yl)-1H-isochromen-1-one (**15**).* The title compound was synthesized according to the general procedure A, starting from (*S*)-3-(1-(4-amino-3-iodo-1*H*-pyrazolo[3,4-*d*]pyrimidin-1-yl)ethyl)-4-(1-((1-ethyl-3,5-dimethyl-1*H*-pyrazol-4-yl)sulfonyl)-1,2,3,6-tetrahydropyridin-4-yl)-1*H*-isochromen-1-one (96 mg, 0.137 mmol) and (3-fluoro-5-hydroxyphenyl)boronic acid (43 mg, 0.274 mmol). Yield 43% (40.5 mg, 0.059 mmol). UPLC−MS (method 9), rt 1.04 min, $[M+H]^+$ 685.4. ^{1}H-NMR (DMSO-d6, 400MHz, mixture of diastereoisomers): δ 10.2 (s, 1H), 8.20-8.13 (m, 1H), 7.99-7.77 (m, 2H), 7.65-7.59 (m, 1H), 7.35 (d, 1H), 6.91-6.79 (m, 2H), 6.69-6.61 (m, 1H), 6.15-5.94 (m, 2H), 4.21-4.04 (m, 3H), 3.88-3.80 (m, 1H), 3.68-3.19 (m, 3H), 2.91-2.84 (m, 1H), 2.78-2.70 (m, 1H), 2.45 (s, 3H), 2.33 (s, 3H), 2.07-1.98 (m, 1H), 1.86-1.75 (m, 3H), 1.39-1.30 (m, 3H).

*(S)-3-(1-(4-amino-3-(3-fluoro-5-hydroxyphenyl)-1H-pyrazolo[3,4-d]pyrimidin-1-yl)ethyl)-4-(1,2,5,6-tetrahydropyridin-3-yl)-1H-isochromen-1-one (**19**)*. A mixture of (*S*)-tert-butyl 3-(3-(1-(4-amino-3-iodo-1*H*-pyrazolo[3,4-*d*]pyrimidin-1-yl)ethyl)-1-oxo-1*H*-isochromen-4-yl)-5,6-dihydropyridine-1(2*H*)-carboxylate (500 mg, 0.814 mmol), 3-fluoro-5-hydroxyphanylboronic acid (254 mg, 1.628 mmol), SPhos Pd G2 (88 mg, 0.122 mmol) and K_3PO_4 (518 mg, 2.441 mmol) in THF/water 3:1 (8 mL) was heated at 80 °C under MW irradiation for 45 min. The reaction was partitioned between water and dichloromethane. The aqueous layer was further extracted with dichloromethane. Combined organic layers were dried over sodium sulfate, filtered and concentrated under reduced pressure. The residue was taken up in MeOH (4 mL) and treated with 4.0 M HCl in 1,4-dioxane (4 mL). Stirring went on until complete cleavage of Boc protecting group, then volatiles were removed under reduced pressure. Fractions collected from reversed phase chromatography (Biotage Isolera, 30 g C18 cartridge, gradient elution from 100:0 to 75:25 A/B, A: water/MeCN 95:5 + 0.1% HCOOH, B: water:MeCN 5/95 + 0.1% HCOOH) were concentrated under reduced pressure. The residue was dissolved in MeOH (4 mL) and stirred in the presence of PL-HCO3 resin. Filtration and concentration under reduced pressure yielded title compound (114 mg, 0.229 mmol, 28.1 % yield) as a white powder. UPLC-MS (method 16), rt 0.54 min, [M+H]+ 498.8. ^{1}H NMR (400 MHz, DMSO-d6) δ ppm 8.22 - 8.30 (m, 1 H), 8.06 - 8.21 (m, 1 H), 7.87 (t, J=7.7 Hz, 1 H), 7.47 - 7.69 (m, 3 H), 6.76 - 7.04 (m, 2 H), 6.66 (d, J=11.0 Hz, 1 H), 6.27 (d, J=7.0 Hz, 1 H), 6.02 (br. s., 1 H), 3.11 - 3.21 (m., 2 H), 2.64 - 3.00 (m, 2 H), 2.19 (d, J=13.2 Hz, 2 H), 1.75 - 1.94 (m, 3 H). ^{13}C NMR (151 MHz, DMSO-d_6) δ ppm 164.02 (1 C, s), 161.67 (1 C, d, *J*=226.70 Hz), 160.82 (1 C, s), 159.50 (1 C, s), 159.46 (1 C, s), 159.41 (1 C, s), 159.38 (1 C, s), 158.00 (1 C, s), 155.71 (1 C, s), 155.71 (1 C, s), 154.03 (1 C, s), 153.69 (1 C, s), 149.89 (1 C, s), 149.60 (1 C, s), 143.01 (1 C, s), 143.01 (1 C, s), 137.00 (1 C,

s), 136.89 (1 C, s), 135.45 (1 C, s), 135.17 (1 C, s), 135.10 (1 C, s), 131.49 (1 C, s), 129.59 (1 C, s), 129.04 (1 C, s), 129.00 (1 C, s), 128.87 (1 C, s), 128.81 (1 C, s), 124.96 (1 C, s), 124.84 (1 C, s), 120.06 (1 C, s), 120.00 (1 C, s), 116.79 (1 C, s), 116.26 (1 C, s), 111.44 (1 C, s), 111.40 (1 C, s), 105.63 (1 C, d, *J*=22.01 Hz), 102.95 (1 C, d, *J*=23.66 Hz), 97.30 (1 C, s), 97.17 (1 C, s), 51.40 (1 C, s), 50.93 (1 C, s), 47.54 (1 C, s), 47.11 (1 C, s), 41.53 (1 C, s), 41.50 (1 C, s), 25.20 (1 C, s), 25.16 (1 C, s), 17.92 (1 C, s), 17.82 (1 C, s).

*(S)-3-(1-(4-amino-3-(3-fluoro-5-hydroxyphenyl)-1H-pyrazolo[3,4-d]pyrimidin-1-yl)ethyl)-4-(1-(2-(1,1-dioxidothiomorpholino)ethyl)-1,2,5,6-tetrahydropyridin-3-yl)-1H-isochromen-1-one (**20**)*.

The title compound was synthesized according to the general procedure A, starting from (*S*)-3-(1-(4-amino-3-iodo-1*H*-pyrazolo[3,4-*d*]pyrimidin-1-yl)ethyl)-4-(1-(2-(1,1-dioxidothiomorpholino)ethyl)-1,2,5,6-tetrahydropyridin-3-yl)-1*H*-isochromen-1-one (4.627 g, 6.849 mmol) and (3-fluoro-5-hydroxyphenyl)boronic acid (2.136 g, 13.698 mmol). Yield 48% (2.17 g, 3.29 mmol). UPLC−MS (method 10), rt 0.59 min, $[M+H]^+$ 660.29. ^{1}H NMR (400 MHz, DMSO-d_6) δ ppm 9.96-10.56 (m, 1H), 8.22-8.28 (m, 1H), 8.13-8.21 (m, 1H), 7.85-7.94 (m, 1H), 7.59-7.67 (m, 1H), 7.41-7.50 (m, 1H), 6.79-6.94 (m, 2H), 6.59-6.70 (m, 1H), 6.07-6.28 (m, 1H), 5.22-6.03 (m, 1H), 2.53-3.22 (m, 14H), 2.13-2.47 (m, 4H), 1.79-1.91 (m, 3H). ^{13}C NMR (151 MHz, DMSO-d_6) δ ppm 164.02 (1 C, s), 162.40 (1 C, s), 160.86 (1 C, d, *J*=234.10 Hz), 160.77 (1 C, s), 159.48 (1 C, s), 159.44 (1 C, s), 159.40 (1 C, s), 159.36 (1 C, s), 157.98 (1 C, s), 155.69 (1 C, s), 154.03 (1 C, s), 153.67 (1 C, s), 150.17 (1 C, s), 149.88 (1 C, s), 143.04 (1 C, s), 143.04 (1 C, s), 136.93 (1 C, s), 135.58 (1 C, s), 135.17 (1 C, s), 135.10 (1 C, s), 129.31 (1 C, s), 129.15 (1 C, s), 129.09 (1 C, br s), 129.06 (1 C, s), 128.93 (1 C, s), 128.85 (1 C, s), 128.40 (1 C, s), 127.61 (1 C, s), 124.55 (1 C, s), 124.55 (1 C, s), 120.07 (1 C, s), 119.98 (1 C, s), 116.35 (1 C, s), 115.81 (1 C, s), 111.44 (1 C, s), 111.40 (1 C, s), 105.63 (1 C, d, *J*=23.10 Hz), 103.05 (1 C, d, *J*=24.20

Hz), 102.93 (1 C, d, *J*=24.20 Hz), 97.31 (1 C, s), 97.20 (1 C, s), 55.34 (1 C, s), 55.20 (1 C, s), 55.17 (1 C, s), 54.66 (1 C, s), 52.61 (1 C, s), 52.57 (1 C, s), 51.46 (1 C, s), 51.02 (1 C, s), 50.53 (1 C, s), 50.32 (1 C, s), 49.12 (1 C, s), 48.99 (1 C, s), 25.82 (1 C, s), 25.70 (1 C, s), 17.89 (1 C, s), 17.76 (1 C, s).

*(S)-3-(1-(4-amino-3-(3-fluoro-5-hydroxyphenyl)-1H-pyrazolo[3,4-d]pyrimidin-1-yl)ethyl)-4-(1-(3-(dimethylamino)-2,2-dimethylpropyl)-1,2,5,6-tetrahydropyridin-3-yl)-1H-isochromen-1-one formate (**21**).* The title compound was synthesized according to the general procedure A, starting from (*S*)-3-(1-(4-amino-3-iodo-1*H*-pyrazolo[3,4-*d*]pyrimidin-1-yl)ethyl)-4-(1-(3-(dimethylamino)-2,2-dimethylpropyl)-1,2,5,6-tetrahydropyridin-3-yl)-1*H*-isochromen-1-one (0.095 g, 0.151 mmol), (3-fluoro-5-hydroxyphenyl)boronic acid (0.047 g, 0.302 mmol). Yield 44% (0.074 g, 0.112 mmol). UPLC−MS (method 9), rt 0.58 min, $[M+H]^+$ 612.4. ^{1}H-NMR (CD_3OD, 400MHz, mixture of diastereoisomers): δ 8.53 (s, 1H), 8.33-8.25 (m, 2H), 7.89-7.81 (m, 1H), 7.66-7.53 (m, 2H), 6.97-6.86 (m, 2H), 6.70-6.63 (m, 1H), 6.31-6.12 (m, 2H), 3.50-2.30 (m, 14H), 2.04-1.92 (m, 3H), 1.20-1.14 (m, 3H), 1.10-1.00 (m, 3H).

*(S)-3-(1-(4-amino-3-(3-fluoro-5-hydroxyphenyl)-1H-pyrazolo[3,4-d]pyrimidin-1-yl)ethyl)-4-(1-((3-((dimethylamino)methyl)oxetan-3-yl)methyl)-1,2,5,6-tetrahydropyridin-3-yl)-1H-isochromen-1-one (**22**).* The title compound was synthesized according to the general procedure A, starting from (*S*)-3-(1-(4-amino-3-iodo-1*H*-pyrazolo[3,4-*d*]pyrimidin-1-yl)ethyl)-4-(1-((3-((dimethylamino)methyl)oxetan-3-yl)methyl)-1,2,5,6-tetrahydropyridin-3-yl)-1*H*-isochromen-1-one (0.200 g, 0.312 mmol), (3-fluoro-5-hydroxyphenyl)boronic acid (0.097 g, 0.623 mmol). Yield 59% (0.116 g, 0.185 mmol). UPLC−MS (method 15), rt 0.96 min, $[M+H]^+$ 626.5. ^{1}H-NMR (DMSO, 400MHz, mixture of diastereoisomers): δ 10.20 (s, 1H), 8.23-8.27 (m, 1H), 8.20-8.14 (m, 1H), 7.91-7.84 (m, 1H), 7.66-7.60 (t, 1H), 7.49-7.40 (m, 1H), 6.93-6.87 (d, 1H), 6.86-

6.80 (m, 1H), 6.70-6.62 (m, 1H), 6.24-6.10 (m, 1H), 6.0 (s, 1H), 4.35-4.17 (m, 4H), 3.25-2.12 (m, 6H), 2.09 (s, 3H), 2.04 (s, 3H), 1.90-1.81 (m, 3H).

*(S)-3-(1-(4-amino-3-(5-hydroxypyridin-3-yl)-1H-pyrazolo[3,4-d]pyrimidin-1-yl)ethyl)-4-(1-((3,5-dimethylisoxazol-4-yl)sulfonyl)-1,2,5,6-tetrahydropyridin-3-yl)-1H-isochromen-1-one (**23**).* The title compound was synthesized according to the general procedure A, starting from (*S*)-3-(1-(4-amino-3-iodo-1*H*-pyrazolo[3,4-*d*]pyrimidin-1-yl)ethyl)-4-(1-((3,5-dimethylisoxazol-4-yl)sulfonyl)-1,2,5,6-tetrahydropyridin-3-yl)-1*H*-isochromen-1-one (2.50 g, 3.712 mmol) and 5-(tetramethyl-1,3,2-dioxaborolan-2-yl)pyridin-3-ol (1.64 g, 7.424 mmol). Yield 48% (1.11 g, 1.74 mmol). UPLC−MS (method 11), rt 0.87 min, $[M+H]^+$ 641.2. ^{1}H NMR (400 MHz DMSO-d_6) δ ppm 10.08-10.54 (m, 1H), 7.84-8.35 (m, 5H), 7.60-7.69 (m, 1H), 7.34-7.51 (m, 2H), 5.34-6.24 (m, 2H), 3.55-3.99 (m, 3H), 3.08-3.24 (m, 1H), 1.93-2.69 (m, 8H), 1.76-1.92 (m, 3H).

*(S)-3-(1-(4-amino-3-(3-fluoro-5-hydroxyphenyl)-1H-pyrazolo[3,4-d]pyrimidin-1-yl)ethyl)-4-(1-((2-(4-methylpiperazin-1-yl)ethyl)sulfonyl)-1,2,5,6-tetrahydropyridin-3-yl)-1H-isochromen-1-one formate (**24**).* The title compound was synthesized according to the general procedure A, starting from (*S*)-3-(1-(4-amino-3-iodo-1*H*-pyrazolo[3,4-*d*]pyrimidin-1-yl)ethyl)-4-(1-((2-(4-methylpiperazin-1-yl)ethyl)sulfonyl)-1,2,5,6-tetrahydropyridin-3-yl)-1*H*-isochromen-1-one (0.1 g, 0.142 mmol) and (3-fluoro-5-hydroxyphenyl)boronic acid (0.044 g, 0.284 mmol). Yield 55% (0.058 g, 0.078 mmol). UPLC−MS (method 13), rt 0.68 min, $[M+H]^+$ 689.3. ^{1}H NMR (400 MHz DMSO-d_6) δ ppm 8.10-8.31 (m, 3H), 7.85-7.95 (m, 1H), 7.59-7.73 (m, 1H), 7.39-7.59 (m, 1H), 6.79-7.00 (m, 2H), 6.61-6.72 (m, 1H), 5.29-6.28 (m, 2H), 2.26-4.21 (m, 18H), 2.16-2.24 (m, 3H), 1.80-1.97 (m, 3H).

*(S)-3-(1-(4-amino-3-(3-fluoro-5-hydroxyphenyl)-1H-pyrazolo[3,4-d]pyrimidin-1-yl)ethyl)-4-(1,2,3,6-tetrahydropyridin-4-yl)-1H-isochromen-1-one hydrochloride (**25**).* To a solution of *tert*-

butyl (*S*)-4-(3-(1-(4-amino-3-(3-fluoro-5-methoxyphenyl)-1*H*-pyrazolo[3,4-*d*]pyrimidin-1-yl)ethyl)-1-oxo-1H-isochromen-4-yl)-3,6-dihydropyridine-1(2*H*)-carboxylate (0.117 g, 0.191 mmol) in dry DCM (2 mL), 1 M BBr_3 in DCM (4.58 mL, 4.58 mmol) was added and the solution was stirred at room temperature for 2.5 h. The solution was cooled to 0 °C and 8 mL of ethanol were added. The solution was evaporated to dryness and crude was purified by flash chromatography Snap C18 12g eluent from H_2O (0.1% HCOOH) to H_2O/MeCN 75/25 (0.1% HCOOH) affording the desired product as a white powder. Then 1.25 M HCl in Methanol (2 mL) was added and the mixture was stirred for 30 minutes. The solution was evaporated to dryness and the product was obtained as a white solid as hydrochloride salt (0.090 g, 0.168 mmol, 88% yield). Chiral HPLC (method A11), rt 4.9 min, e.e.>99%. UPLC−MS (method 13), rt 0.63 min, $[M+H]^+$ 499.3. ^{1}H NMR (400 MHz, DMSO-d_6) δ ppm 10.18-10.43 (m, 1H), 8.97-9.31 (m, 2H), 8.25-8.46 (m, 1H), 8.10-8.24 (m, 1H), 7.83-7.98 (m, 1H), 7.60-7.81 (m, 2H), 6.81-7.00 (m, 2H), 6.63-6.78 (m, 1H), 6.11-6.26 (m, 1H), 5.55-6.11 (m, 1H), 2.54-3.93 (m, 6H), 1.85-1.99 (m, 3H).

*(S)-3-(1-(4-amino-3-(3-fluoro-5-hydroxyphenyl)-1H-pyrazolo[3,4-d]pyrimidin-1-yl)ethyl)-4-(1-(pyrazin-2-ylmethyl)-1,2,3,6-tetrahydropyridin-4-yl)-1H-isochromen-1-one (**26**)*. The title compound was synthesized according to the general procedure A, starting from (*S*)-3-(1-(4-amino-3-iodo-1*H*-pyrazolo[3,4-*d*]pyrimidin-1-yl)ethyl)-4-(1-(pyrazin-2-ylmethyl)-1,2,3,6-tetrahydropyridin-4-yl)-1*H*-isochromen-1-one (0.510 g, 0.841 mmol) and (3-fluoro-5-hydroxyphenyl)boronic acid (0.260 g, 1.68 mmol). Yield 36% (0.180 g, 0.305 mmol). UPLC−MS (method 11), rt 0.58 min, $[M+H]^+$ 5912. ^{1}H-NMR (DMSO, 400MHz, mixture of diastereoisomers): δ 10.2 (s, 1H), 8.81 (s, 1H), 8.62 (s, 1H), 8.58 (t, 1H), 8.24 (s, 1H), 8.21-8.14 (m, 2H), 7.92-7.86 (m, 1H), 7.66-7.60 (m, 1H), 7.5-7.43 (m, 1H), 6.93-6.87 (m, 1H), 6.87-6.79

(m, 1H), 6.68-6.60 (m, 1H), 6.27-6.07 (m, 1H), 5.99 (br s, 1H), 3.90-3.77 (m, 2H), 3.24-2.20 (m, 6H), 1.91-1.80 (m, 3H).

*(S)-3-(1-(4-amino-3-(3-fluoro-5-hydroxyphenyl)-1H-pyrazolo[3,4-d]pyrimidin-1-yl)ethyl)-4-(1-(methylsulfonyl)-1,2,3,6-tetrahydropyridin-4-yl)-1H-isochromen-1-one (**27**).* The title compound was synthesized according to the general procedure A, starting from (*S*)-3-(1-(4-amino-3-iodo-1*H*-pyrazolo[3,4-*d*]pyrimidin-1-yl)ethyl)-4-(1-(methylsulfonyl)-1,2,3,6-tetrahydropyridin-4-yl)-1*H*-isochromen-1-one (0.079 g, 0.13 mmol) and (3-fluoro-5-hydroxyphenyl)boronic acid (0.041 g, 0.26 mmol). Yield 15% (0.011 g, 0.019 mmol). UPLC−MS (method 12), rt 0.82 min, $[M+H]^+$ 577.3. ^{1}H NMR (400 MHz, DMSO-d_6) δ ppm 8.13-8.30 (m, 2H), 7.82-7.92 (m, 1H), 7.58-7.69 (m, 1H), 7.39-7.51 (m, 1H), 6.59-6.94 (m, 3H), 5.31-6.23 (m, 2H), 3.45-3.82 (m, 4H), 2.99-3.07 (m, 3H), 2.34-2.47 (m, 2H), 1.80-1.95 (m, 3H).

Molecular modeling.

Protein preparation and docking grids. The X-ray structure of human PI3Kδ co-crystallized with a selective small-molecule inhibitor was retrieved from the Protein Data Bank (PDB: 6G6W)[39] and subsequently processed using the Protein Preparation Wizard tool[40] of Maestro. Briefly, missing hydrogen atoms were added to the protein-ligand complex and protein C- and N-termini were capped with acetyl and methylamino groups, respectively. Missing side chains were reconstructed with Prime,[41,42] while the hydrogen bond (H-bond) network was optimized by sampling the orientation of polar side chains as well as the tautomerization states of histidine. Subsequently, all hydrogens were energy minimized to further refine the optimized H-bond network. A final energy minimization was conducted to relieve major steric clashes, retaining all hydrogens free to move while restraining all heavy atoms with a harmonic potential of 25 kcal mol^{-1} $Å^{-2}$. All water molecules were removed from the final energy-minimized structure.

Docking grids were built with Glide[43] and centered on the co-crystallized ligand molecule, retaining default values for enclosing and bounding box dimensions as well as for the van der Waals scaling factor.

Ligand docking. Compounds **7** and **9** were built with Maestro and subsequently subjected to a conformational search with the ConfGenX[44] utility of Schrodinger, retaining up to 200 conformers. The resulting ligand geometries were placed at random positions in the 3D space and docked within the ATP-binding site of PI3Kδ, applying default settings. The canonicalization of the input ligand structure was de-activated during docking calculations and one docking pose was retained for each conformer. Only the top-ranked pose according to the Emodel score was selected for each compound.

ASSOCIATED CONTENT

Supporting Information.

The Supporting Information is available free of charge via the Internet at http://pubs.acs.org. Table S1: Summary of crystallographic data of hPI3Kδ in complex with compounds **10** and **18** and hPI3Kγ in complex with compound **10**; Table S2: kinome selectivity of CHF-6523 (**18**) in the scanMAX KINOMEscan® profiling panel; Table S3: off-target selectivity of CHF-6523 (**18**) in the LeadProfilingScreen panel; experimental procedures for the synthesis of intermediates; experimental procedures for the synthesis of compound **18** (CHF-6523); NMR spectra and HPLC traces of final compounds (PDF). Compound molecular formula string with *in vitro* pharmacology, PhysChem and ADME data tables (CSV).

Accession Codes.

PDB accession codes: compound **10** bound to hPI3Kδ (9GDI), compound **11** bound to hPI3Kγ (9GG9), compound **18** (CHF-6523) bound to hPI3Kδ (9GCF).

AUTHOR INFORMATION

Corresponding Authors

*Paolo Bruno – Chiesi Farmaceutici S.p.A., Nuovo Centro Ricerche, Largo Belloli 11/a, 43122, Parma, Italy; e-mail: p.bruno@chiesi.com.

*Matteo Biagetti – Chiesi Farmaceutici S.p.A., Nuovo Centro Ricerche, Largo Belloli 11/a, 43122, Parma, Italy; e-mail: m.biagetti@chiesi.com.

Author Contributions

Paolo Bruno, Daniele Pala, Alessandra Micoli and Mauro Corsi contributed equally. All authors have given approval to the final version of the manuscript.

Funding Sources

The research was supported by Ministero dello Sviluppo Economico Fondo Crescita Sostenibile Accordi per l'Innovazione DM 24.05.2017 (Project N. F/130013/00/X38).

Notes

The authors declare the following competing financial interest(s): all authors were employees and/or shareholders of Chiesi Farmaceutici S.p.A. or Aptuit, an Evotec Company when this work was carried out.

ACKNOWLEDGMENTS

We thank Proteros Biostructures GmbH, Planegg-Martinsried, Germany, for solving the crystal structure of human PI3Kδ in complex with compounds **10** (PDB code 9GDI) and **18** (CHF-6523, PDB code 9GCF), and of human PI3Kγ in complex with compound **11** (PDB code 9GG9) and Dr. Doriano Lamba for his excellent contribution to the analysis of the crystallographic results. We also thank Daniel Pecorari (Chiesi Analytics & Early Formulations Department) for outstanding support in processing NMR data and Stefano Zilocchi (Chiesi Compound Management Unit) for the invaluable support to this and all preclinical drug discovery projects.

ABBREVIATIONS

ACN, acetonitrile; ADP, adenosine diphosphate; Asp, aspartate; ATP, adenosine triphosphate; AUC, area under the curve; Boc, tert-butyloxycarbonyl; ^{t}Bu, tert-butyl; BSA, bovine serum albumin; CLi, intrinsic clearance; CYP450, cytochrome p450; DCM, dichloromethane; DIPEA, *N*,*N*-diisopropylethylamine; DMAP, 4-dimethylaminopyridine; DMF, dimethylformamide; DMSO, dimethylsulfoxide; DP, dry powder; dppf, 1,1'-bis(diphenylphosphino) ferrocene; DTT, dithiothreitol; EGTA, egtazic acid; FBS, fetal bovine serum; GLP, good laboratory practice; HBSS, Hank's balanced salt solutions; hERG, human ether-a-go-go related gene; HPLC, high pressure liquid chromatography; IC, inhibitory concentration; LC-MS, liquid chromatography/mass spectrometry; M, molar/molarity; MEM, minumum essential medium; min, minute/mins; MS, mass spectrometry; MW, microwave; NADPH, nicotinamide adenine dinucleotide phosphate; NMR, nuclear magnetic resonance; NOAEL, no observed adverse effect level; NOEL, no-observed-effect level; OVA, ovalbumin; P_{app} AB, apical to basolateral apparent permeability; PBPK, physiologically based pharmacokinetic; PBS, phosphate-buffered saline; PDB, Protein Data Bank; P-gp, P-glycoprotein; PI3K, phosphatidylinositol 3-kinase, QC, quality control; r.t., room temperature; RLU, relative light unit; rt, retention time; SPhos Pd G2, chloro(2-dicyclohexylphosphino-2',6'-dimethoxy-11'-biphenyl)2-(2-amino-1,1'-biphenyl)palladium(II); TEA, triethylamine; THF, tetrahydrofuran; TPSA, topological polar surface area; Tyr, tyrosine; UDPGA, uridine diphosphate glucuronic acid; UPLC, ultra

performance liquid chromatography; UPLC, ultra performance liquid chromatography-mass spectrometry; XPhos, dicyclohexyl[2′,4′,6′-tris(propan-2-yl)[1,1′-biphenyl]-2-yl]phosphane.

REFERENCES

(1) Web-Site: Https://Ginasthma.Org/Pocket-Guide-for-Asthma-Management-and-Prevention/ (Accessed May, 6th 2024). https://ginasthma.org/pocket-guide-for-asthma-management-and-prevention/.
(2) Web-Site: Https://Goldcopd.Org/2024-Gold-Report/ (Accessed May, 6th 2024).
(3) Barnes, P. J.; Shapiro, S. D.; Pauwels, R. A. Chronic Obstructive Pulmonary Disease: Molecular and Cellularmechanisms. *Eur Respir J* **2003**, *22* (4), 672–688. https://doi.org/10.1183/09031936.03.00040703.
(4) Barnes, P. J. Corticosteroid Resistance in Patients with Asthma and Chronic Obstructive Pulmonary Disease. *Journal of Allergy and Clinical Immunology* **2013**, *131* (3), 636–645. https://doi.org/10.1016/j.jaci.2012.12.1564.
(5) Ito, K.; Caramori, G.; Adcock, I. M. Therapeutic Potential of Phosphatidylinositol 3-Kinase Inhibitors in Inflammatory Respiratory Disease. *J Pharmacol Exp Ther* **2007**, *321* (1), 1–8. https://doi.org/10.1124/jpet.106.111674.
(6) Marwick, J. A.; Caramori, G.; Stevenson, C. S.; Casolari, P.; Jazrawi, E.; Barnes, P. J.; Ito, K.; Adcock, I. M.; Kirkham, P. A.; Papi, A. Inhibition of PI3Kδ Restores Glucocorticoid Function in Smoking-Induced Airway Inflammation in Mice. *Am. J. Respir. Crit. Care Med.* **2009**, *179*, 542–548. https://doi.org/10.1164/rccm.200810-1570OC.
(7) Barnes, P. J. Mechanisms and Resistance in Glucocorticoid Control of Inflammation. *The Journal of Steroid Biochemistry and Molecular Biology* **2010**, *120* (2–3), 76–85. https://doi.org/10.1016/j.jsbmb.2010.02.018.
(8) Marwick, J. A.; Caramori, G.; Casolari, P.; Mazzoni, F.; Kirkham, P. A.; Adcock, I. M.; Chung, K. F.; Papi, A. A Role for Phosphoinositol 3–Kinase δ in the Impairment of Glucocorticoid Responsiveness in Patients with Chronic Obstructive Pulmonary Disease. *Journal of Allergy and Clinical Immunology* **2010**, *125* (5), 1146–1153. https://doi.org/10.1016/j.jaci.2010.02.003.
(9) To, Y.; Ito, K.; Kizawa, Y.; Failla, M.; Ito, M.; Kusama, T.; Elliott, W. M.; Hogg, J. C.; Adcock, I. M.; Barnes, P. J. Targeting Phosphoinositide-3-Kinase-δ with Theophylline Reverses Corticosteroid Insensitivity in Chronic Obstructive Pulmonary Disease. *Am J Respir Crit Care Med* **2010**, *182* (7), 897–904. https://doi.org/10.1164/rccm.200906-0937OC.
(10) Durham, A. L.; Caramori, G.; Chung, K. F.; Adcock, I. M. Targeted Anti-Inflammatory Therapeutics in Asthma and Chronic Obstructive Lung Disease. *Translational Research* **2016**, *167* (1), 192–203. https://doi.org/10.1016/j.trsl.2015.08.004.
(11) Stokes, C. A.; Condliffe, A. M. Phosphoinositide 3-Kinase δ (PI3Kδ) in Respiratory Disease. *Biochemical Society Transactions* **2018**, *46* (2), 361–369. https://doi.org/10.1042/BST20170467.
(12) Fruman, D. A.; Chiu, H.; Hopkins, B. D.; Bagrodia, S.; Cantley, L. C.; Abraham, R. T. The PI3K Pathway in Human Disease. *Cell* **2017**, *170* (4), 605–635. https://doi.org/10.1016/j.cell.2017.07.029.
(13) Milara, J.; Lluch, J.; Almudever, P.; Freire, J.; Xiaozhong, Q.; Cortijo, J. Roflumilast N-Oxide Reverses Corticosteroid Resistance in Neutrophils from Patients with Chronic

Obstructive Pulmonary Disease. *Journal of Allergy and Clinical Immunology* **2014**, *134* (2), 314-322.e9. https://doi.org/10.1016/j.jaci.2014.02.001.

(14) Angulo, I.; Vadas, O.; Garçon, F.; Banham-Hall, E.; Plagnol, V.; Leahy, T. R.; Baxendale, H.; Coulter, T.; Curtis, J.; Wu, C.; Blake-Palmer, K.; Perisic, O.; Smyth, D.; Maes, M.; Fiddler, C.; Juss, J.; Cilliers, D.; Markelj, G.; Chandra, A.; Farmer, G.; Kielkowska, A.; Clark, J.; Kracker, S.; Debré, M.; Picard, C.; Pellier, I.; Jabado, N.; Morris, J. A.; Barcenas-Morales, G.; Fischer, A.; Stephens, L.; Hawkins, P.; Barrett, J. C.; Abinun, M.; Clatworthy, M.; Durandy, A.; Doffinger, R.; Chilvers, E. R.; Cant, A. J.; Kumararatne, D.; Okkenhaug, K.; Williams, R. L.; Condliffe, A.; Nejentsev, S. Phosphoinositide 3-Kinase δ Gene Mutation Predisposes to Respiratory Infection and Airway Damage. *Science* **2013**, *342* (6160), 866–871. https://doi.org/10.1126/science.1243292.

(15) Lucas, C. L.; Kuehn, H. S.; Zhao, F.; Niemela, J. E.; Deenick, E. K.; Palendira, U.; Avery, D. T.; Moens, L.; Cannons, J. L.; Biancalana, M.; Stoddard, J.; Ouyang, W.; Frucht, D. M.; Rao, V. K.; Atkinson, T. P.; Agharahimi, A.; Hussey, A. A.; Folio, L. R.; Olivier, K. N.; Fleisher, T. A.; Pittaluga, S.; Holland, S. M.; Cohen, J. I.; Oliveira, J. B.; Tangye, S. G.; Schwartzberg, P. L.; Lenardo, M. J.; Uzel, G. Dominant-Activating Germline Mutations in the Gene Encoding the PI(3)K Catalytic Subunit P110δ Result in T Cell Senescence and Human Immunodeficiency. *Nat Immunol* **2014**, *15* (1), 88–97. https://doi.org/10.1038/ni.2771.

(16) Stark, A.-K.; Chandra, A.; Chakraborty, K.; Alam, R.; Carbonaro, V.; Clark, J.; Sriskantharajah, S.; Bradley, G.; Richter, A. G.; Banham-Hall, E.; Clatworthy, M. R.; Nejentsev, S.; Hamblin, J. N.; Hessel, E. M.; Condliffe, A. M.; Okkenhaug, K. PI3Kδ Hyper-Activation Promotes Development of B Cells That Exacerbate Streptococcus Pneumoniae Infection in an Antibody-Independent Manner. *Nat Commun* **2018**, *9* (1), 3174. https://doi.org/10.1038/s41467-018-05674-8.

(17) Sapey, E.; Stockley, J. A.; Greenwood, H.; Ahmad, A.; Bayley, D.; Lord, J. M.; Insall, R. H.; Stockley, R. A. Behavioral and Structural Differences in Migrating Peripheral Neutrophils from Patients with Chronic Obstructive Pulmonary Disease. *Am J Respir Crit Care Med* **2011**, *183* (9), 1176–1186. https://doi.org/10.1164/rccm.201008-1285OC.

(18) Stark, A.-K.; Sriskantharajah, S.; Hessel, E. M.; Okkenhaug, K. PI3K Inhibitors in Inflammation, Autoimmunity and Cancer. *Current Opinion in Pharmacology* **2015**, *23*, 82–91. https://doi.org/10.1016/j.coph.2015.05.017.

(19) Stark, A.-K.; Chandra, A.; Chakraborty, K.; Alam, R.; Carbonaro, V.; Clark, J.; Sriskantharajah, S.; Bradley, G.; Richter, A. G.; Banham-Hall, E.; Clatworthy, M. R.; Nejentsev, S.; Hamblin, J. N.; Hessel, E. M.; Condliffe, A. M.; Okkenhaug, K. PI3Kδ Hyper-Activation Promotes Development of B Cells That Exacerbate Streptococcus Pneumoniae Infection in an Antibody-Independent Manner. *Nat Commun* **2018**, *9* (1), 3174. https://doi.org/10.1038/s41467-018-05674-8.

(20) Wei, J.; Gu, D.; Yuan, L.; Sheng, R. Advances in the Discovery of Novel Inhaled PI3Kδ Inhibitors for theTreatment of Asthma. *CMC* **2023**, *30* (17), 1971–1992. https://doi.org/10.2174/0929867329666220819115011.

(21) Perry, M. W. D.; Abdulai, R.; Mogemark, M.; Petersen, J.; Thomas, M. J.; Valastro, B.; Westin Eriksson, A. Evolution of PI3Kγ and δ Inhibitors for Inflammatory and Autoimmune Diseases. *J. Med. Chem.* **2019**, *62* (10), 4783–4814. https://doi.org/10.1021/acs.jmedchem.8b01298.

(22) U.S. Food and Drug Administration. FDA Briefing Document. Oncologic Drugs Advisory Committee Meeting. April 21, 2022. Phosphatidylinositol 3-Kinase (PI3K) Inhibitors in Hematologic Malignancies, 2022. https://fda.report/media/157762/ODAC-20220421-Backgrounder-FDA.pdf (accessed 2024-05-10).
(23) Burke, J. E.; Triscott, J.; Emerling, B. M.; Hammond, G. R. V. Beyond PI3Ks: Targeting Phosphoinositide Kinases in Disease. *Nat Rev Drug Discov* **2023**, *22* (5), 357–386. https://doi.org/10.1038/s41573-022-00582-5.
(24) Khan, K. H.; Wong, M.; Rihawi, K.; Bodla, S.; Morganstein, D.; Banerji, U.; Molife, L. R. Hyperglycemia and Phosphatidylinositol 3-Kinase/Protein Kinase B/Mammalian Target of Rapamycin (PI3K/AKT/mTOR) Inhibitors in Phase I Trials: Incidence, Predictive Factors, and Management. *The Oncologist* **2016**, *21* (7), 855–860. https://doi.org/10.1634/theoncologist.2015-0248.
(25) Laurent, P.-A.; Séverin, S.; Hechler, B.; Vanhaesebroeck, B.; Payrastre, B.; Gratacap, M.-P. Platelet PI3Kβ and GSK3 Regulate Thrombus Stability at a High Shear Rate. *Blood* **2015**, *125* (5), 881–888. https://doi.org/10.1182/blood-2014-07-588335.
(26) Berndt, A.; Miller, S.; Williams, O.; Le, D. D.; Houseman, B. T.; Pacold, J. I.; Gorrec, F.; Hon, W.-C.; Ren, P.; Liu, Y.; Rommel, C.; Gaillard, P.; Rückle, T.; Schwarz, M. K.; Shokat, K. M.; Shaw, J. P.; Williams, R. L. The P110δ Structure: Mechanisms for Selectivity and Potency of New PI(3)K Inhibitors. *Nat Chem Biol* **2010**, *6* (2), 117–124. https://doi.org/10.1038/nchembio.293.
(27) Bruno, P.; Micoli, A.; Corsi, M.; Pala, D.; Guariento, S.; Fiorelli, C.; Ronchi, P.; Fioni, A.; Gallo, P. M.; Marenghi, G.; Bertolini, S.; Capacchi, S.; Mileo, V.; Biagetti, M.; Capelli, A. M. Discovery and Optimization of Pyridazinones as PI3Kδ Selective Inhibitors for Administration by Inhalation. *J. Med. Chem.* **2024**, *67* (13), 11103–11124. https://doi.org/10.1021/acs.jmedchem.4c00610.
(28) Mazzucato, R.; Roberti, M.; Capelli, A. M.; Rancati, F.; Biagetti, M.; Fiorelli, C.; Bruno, P.; Ronchi, P.; Bertolini, S.; Corsi, M.; Pala, D. Application of an "Inhalation by Design" Approach to the Identification and in-Vitro Evaluation of Novel Purine Based PI3Kδ Inhibitors. *European Journal of Medicinal Chemistry* **2023**, *254*, 115331. https://doi.org/10.1016/j.ejmech.2023.115331.
(29) Williams, O.; Houseman, B. T.; Kunkel, E. J.; Aizenstein, B.; Hoffman, R.; Knight, Z. A.; Shokat, K. M. Discovery of Dual Inhibitors of the Immune Cell PI3Ks P110δ and P110γ: A Prototype for New Anti-Inflammatory Drugs. *Chemistry & Biology* **2010**, *17* (2), 123–134. https://doi.org/10.1016/j.chembiol.2010.01.010.
(30) Lannutti, B. J.; Meadows, S. A.; Herman, S. E. M.; Kashishian, A.; Steiner, B.; Johnson, A. J.; Byrd, J. C.; Tyner, J. W.; Loriaux, M. M.; Deininger, M.; Druker, B. J.; Puri, K. D.; Ulrich, R. G.; Giese, N. A. CAL-101, a P110δ Selective Phosphatidylinositol-3-Kinase Inhibitor for the Treatment of B-Cell Malignancies, Inhibits PI3K Signaling and Cellular Viability. *Blood* **2011**, *117* (2), 591–594. https://doi.org/10.1182/blood-2010-03-275305.
(31) Down, K.; Amour, A.; Baldwin, I. R.; Cooper, A. W. J.; Deakin, A. M.; Felton, L. M.; Guntrip, S. B.; Hardy, C.; Harrison, Z. A.; Jones, K. L.; Jones, P.; Keeling, S. E.; Le, J.; Livia, S.; Lucas, F.; Lunniss, C. J.; Parr, N. J.; Robinson, E.; Rowland, P.; Smith, S.; Thomas, D. A.; Vitulli, G.; Washio, Y.; Hamblin, J. N. Optimization of Novel Indazoles as Highly Potent and Selective Inhibitors of Phosphoinositide 3-Kinase δ for the Treatment of Respiratory Disease. *J. Med. Chem.* **2015**, *58* (18), 7381–7399. https://doi.org/10.1021/acs.jmedchem.5b00767.

(32) Miller, M.; Thompson, P.; Gabelli, S. Structural Determinants of Isoform Selectivity in PI3K Inhibitors. *Biomolecules* **2019**, *9* (3), 82. https://doi.org/10.3390/biom9030082.
(33) Pasqua, E.; Hamblin, N.; Edwards, C.; Baker-Glenn, C.; Hurley, C. Developing Inhaled Drugs for Respiratory Diseases: A Medicinal Chemistry Perspective. *Drug Discovery Today* **2022**, *27* (1), 134–150. https://doi.org/10.1016/j.drudis.2021.09.005.
(34) Begg, M.; Edwards, C. D.; Hamblin, J. N.; Pefani, E.; Wilson, R.; Gilbert, J.; Vitulli, G.; Mallett, D.; Morrell, J.; Hingle, M. I.; Uddin, S.; Ehtesham, F.; Marotti, M.; Harrell, A.; Newman, C. F.; Fernando, D.; Clark, J.; Cahn, A.; Hessel, E. M. Translation of Inhaled Drug Optimization Strategies into Clinical Pharmacokinetics and Pharmacodynamics Using GSK2292767A, a Novel Inhaled Phosphoinositide 3-Kinase *δ* Inhibitor. *J Pharmacol Exp Ther* **2019**, *369* (3), 443–453. https://doi.org/10.1124/jpet.119.257311.
(35) Mairinger, S.; Hernández-Lozano, I.; Filip, T.; Löbsch, M.; Stanek, J.; Zeitlinger, M.; Hacker, M.; Tournier, N.; Wanek, T.; Ehrhardt, C.; Langer, O. Influence of P-Glycoprotein on Pulmonary Disposition of the Model Substrate [11C]Metoclopramide Assessed by PET Imaging in Rats. *European Journal of Pharmaceutical Sciences* **2023**, *183*, 106404. https://doi.org/10.1016/j.ejps.2023.106404.
(36) Perry, M. W. D.; Björhall, K.; Bonn, B.; Carlsson, J.; Chen, Y.; Eriksson, A.; Fredlund, L.; Hao, H.; Holden, N. S.; Karabelas, K.; Lindmark, H.; Liu, F.; Pemberton, N.; Petersen, J.; Rodrigo Blomqvist, S.; Smith, R. W.; Svensson, T.; Terstiege, I.; Tyrchan, C.; Yang, W.; Zhao, S.; Öster, L. Design and Synthesis of Soluble and Cell-Permeable PI3Kδ Inhibitors for Long-Acting Inhaled Administration. *J. Med. Chem.* **2017**, *60* (12), 5057–5071. https://doi.org/10.1021/acs.jmedchem.7b00401.
(37) Robinson, D.; Bertrand, T.; Carry, J.-C.; Halley, F.; Karlsson, A.; Mathieu, M.; Minoux, H.; Perrin, M.-A.; Robert, B.; Schio, L.; Sherman, W. Differential Water Thermodynamics Determine PI3K-Beta/Delta Selectivity for Solvent-Exposed Ligand Modifications. *J. Chem. Inf. Model.* **2016**, *56* (5), 886–894. https://doi.org/10.1021/acs.jcim.5b00641.
(38) Govoni, M.; Bassi, M.; Girardello, L.; Lucci, G.; Rony, F.; Charretier, R.; Galkin, D.; Faietti, M. L.; Pioselli, B.; Modafferi, G.; Benfeitas, R.; Bonatti, M.; Miglietta, D.; Clark, J.; Pedersen, F.; Kirsten, A.-M.; Beeh, K.-M.; Kornmann, O.; Korn, S.; Ludwig-Sengpiel, A.; Watz, H. CHF6523 Data Suggest That the Phosphoinositide 3-Kinase Delta Isoform Is Not a Suitable Target for the Management of COPD. *Respir Res* **2024**, *25* (1), 380. https://doi.org/10.1186/s12931-024-02999-5.
(39) Erra, M.; Taltavull, J.; Bernal, F. J.; Caturla, J. F.; Carrascal, M.; Pagès, L.; Mir, M.; Espinosa, S.; Gràcia, J.; Domínguez, M.; Sabaté, M.; Paris, S.; Maldonado, M.; Hernández, B.; Bravo, M.; Calama, E.; Miralpeix, M.; Lehner, M. D.; Calbet, M. Discovery of a Novel Inhaled PI3Kδ Inhibitor for the Treatment of Respiratory Diseases. *J. Med. Chem.* **2018**, *61* (21), 9551–9567. https://doi.org/10.1021/acs.jmedchem.8b00873.
(40) Madhavi Sastry, G.; Adzhigirey, M.; Day, T.; Annabhimoju, R.; Sherman, W. Protein and Ligand Preparation: Parameters, Protocols, and Influence on Virtual Screening Enrichments. *J Comput Aided Mol Des* **2013**, *27* (3), 221–234. https://doi.org/10.1007/s10822-013-9644-8.
(41) Jacobson, M. P.; Friesner, R. A.; Xiang, Z.; Honig, B. On the Role of the Crystal Environment in Determining Protein Side-Chain Conformations. *Journal of Molecular Biology* **2002**, *320* (3), 597–608. https://doi.org/10.1016/S0022-2836(02)00470-9.

(42) Jacobson, M. P.; Pincus, D. L.; Rapp, C. S.; Day, T. J. F.; Honig, B.; Shaw, D. E.; Friesner, R. A. A Hierarchical Approach to All-atom Protein Loop Prediction. *Proteins* **2004**, *55* (2), 351–367. https://doi.org/10.1002/prot.10613.

(43) Friesner, R. A.; Banks, J. L.; Murphy, R. B.; Halgren, T. A.; Klicic, J. J.; Mainz, D. T.; Repasky, M. P.; Knoll, E. H.; Shelley, M.; Perry, J. K.; Shaw, D. E.; Francis, P.; Shenkin, P. S. Glide: A New Approach for Rapid, Accurate Docking and Scoring. 1. Method and Assessment of Docking Accuracy. *J. Med. Chem.* **2004**, *47* (7), 1739–1749. https://doi.org/10.1021/jm0306430.

(44) Watts, K. S.; Dalal, P.; Murphy, R. B.; Sherman, W.; Friesner, R. A.; Shelley, J. C. ConfGen: A Conformational Search Method for Efficient Generation of Bioactive Conformers. *J. Chem. Inf. Model.* **2010**, *50* (4), 534–546. https://doi.org/10.1021/ci100015j.

For Table of Contents Only